Supporting Information

Six-Coordinate Zinc Porphyrins for Template-Directed Synthesis of Spiro-Fused Nanorings

Ludovic Favereau,[†] Arjen Cnossen,[†] Julien B. Kelber,[†] Juliane Q. Gong,[‡] René M. Oetterli,[†] Jonathan Cremers,[†] Laura M. Herz,[‡] and Harry L. Anderson*[,†]

[†] Department of Chemistry, University of Oxford, Chemistry Research Laboratory, Oxford, OX1 3TA

[‡] Department of Physics, University of Oxford, Clarendon Laboratory, Parks Road, Oxford, OX1 3PU

* harry.anderson@chem.ox.ac.uk

Table of Contents

A. General Methods

All reagents were purchased from commercial sources and solvents were used as supplied unless otherwise noted. Dry solvents ($CHCl_3$, CH_2Cl_2 and toluene) were obtained by passing through alumina under N_2. Diisopropylamine (DIPA) was dried over calcium hydride, distilled and stored under N_2 over molecular sieves. NMR data were recorded at 500 MHz using a Bruker AVII500 (with cryoprobe) or DRX500, or at 400 MHz using a Bruker AVII400 or AVIII400, or at 700 MHz using a Bruker AVIII700 (with cryoprobe) at 298 K. Chemical shifts are quoted as parts per million (ppm) relative to residual $CHCl_3$ (δ_H 7.27 ppm for ^{1}H NMR and at δ_C 77.2 ppm for ^{13}C NMR) and coupling constants (J) are reported in Hertz. MALDI-ToF spectra were measured at the EPSRC National Mass Spectrometry service (Swansea) using the Applied Biosystems Voyager DE-STR or at the University of Oxford using Waters MALDI Micro MX spectrometer (with *trans*-2-[3-(4-*tert*-butylphenyl)-2-methyl-2-propenylidene]malononitrile (DCTB) as matrix). UV/vis/NIR absorbance measurements were recorded at 25 °C with a Perkin-Elmer Lambda 20 photospectrometer using quartz 1 cm cuvettes. UV/vis/NIR titrations were analyzed by calculating the difference in absorptions and plotted using Origin™ software or fitted to models using SPECFIT™ software.[S1] Size exclusion chromatography (SEC) was carried out using Bio-Beads S-X1, 200–400 mesh (BioRad). Analytical and semi-preparative GPC were carried out on Shimadzu Recycling GPC system equipped with LC-20 AD pump, SPD-M20A UV detector and a set of JAIGEL 3H (20 × 600 mm) and JAIGEL 4H (20 × 600 mm) columns in toluene/1% pyridine as eluent with a flow rate of 3.5 mL/min.

B. Synthetic procedures

Tetra-(TIPS-acetylene) zinc octaethylporphyrin **(TIPS)$_4$*x*Et-P1**,[S2] tetra-(TMS-acetylene) zinc porphyrin **(TMS)$_4$*x*-P1**,[S3] porphyrin monomer **P1**[S4] and template **T6**[S5] were prepared using previously reported procedures. The synthesis of linear trimer ***l*-P3$_{THS}$**, cross pentamers ***x*Et-P5** and ***x*-P5** are summarized in Scheme S1.

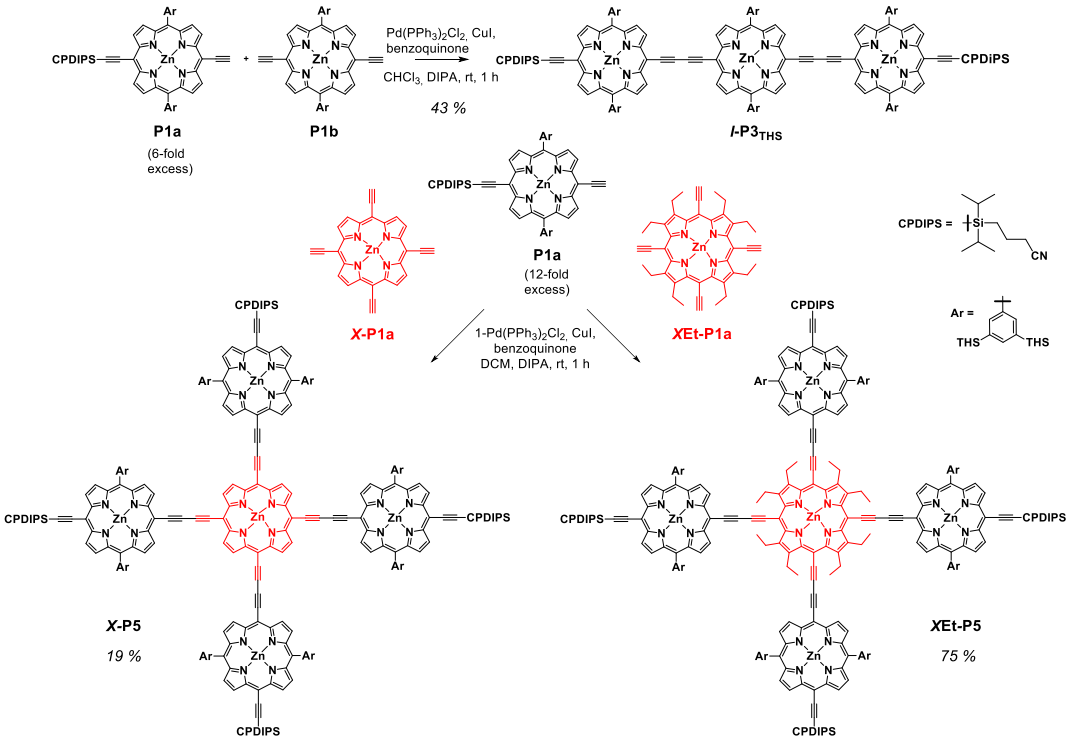

Scheme S1. Syntheses of linear trimer ***l*-P3$_{THS}$**, cross pentamers ***x*Et-P5** and ***x*-P5**. CPDIPS = cyanopropyldiisopropylsilyl. Ar = 3,5-bis(trihexylsilyl)phenyl.

Preparation of *l*-P3$_{THS}$

Mono-deprotected monomer **P1a** (1.01 g, 0.54 mmol) and bis-deprotected **P1b** (153 mg, 0.09 mmol) were dissolved in toluene (15 mL). Then a catalyst solution of $Pd(PPh_3)_2Cl_2$ (6.3 mg, 9.0 μmol), CuI (8.5 mg, 0.05 mmol) and 1,4-benzoquinone (19.4 mg, 0.18 mmol) in a mixture of toluene (7 mL) and distilled DIPA (7 mL) was added and the reaction mixture was stirred at room temperature for 1 h. The solution was passed through a short silica plug (100:1 CH_2Cl_2:pyridine). The crude mixture was purified by column chromatography (4:1 / 40–60 petrol ether: CH_2Cl_2) and size-exclusion chromatography (BioBeads SX-1, toluene) before precipitated using CH_2Cl_2/MeOH to yield ***l*-P3$_{THS}$** (212 mg, 43%) as a dark green solid.

^{1}H NMR (400 MHz, $CDCl_3$, 298 K): δ_H (ppm) 9.99 (d, J = 4.4 Hz, 8H), 9.74 (d, J = 4.4 Hz, 4H), 9.06 (d, J = 4.6 Hz, 4H), 9.04 (d, J = 4.6 Hz, 4H), 8.98 (d, J = 4.5 Hz, 4H), 8.38 (s, 4H), 8.32 (s, 8H), 8.08 (s, 2H), 8.06 (s, 4H), 2.59 (t, J = 6.9 Hz, 4H), 2.28–2.20 (m, 4H), 1.60–1.49 (m, 72H), 1.50–1.39 (m, 96H), 1.39–1.29 (m, 144H), 1.25–1.19 (m, 8H), 1.04–0.95 (m, 72H), 0.95–0.87 (m,108H).
^{13}C NMR (100 MHz, $CDCl_3$, 298 K): δ_C (ppm) 153.2, 152.4, 151.0, 150.8, 150.6, 140.8, 140.5, 140.3, 140.2, 139.5, 135.4, 135.3, 133.6, 133.4, 131.3, 131.2, 125.2, 124.8, 119.8, 110.2, 101.8, 101.0, 100.5, 97.5, 87.7, 87.5, 82.9, 82.7, 33.7, 33.7, 31.8, 31.8, 24.2, 24.2, 22.9, 22.8, 21.8, 21.2, 18.8, 18.5, 14.4, 14.3, 12.8, 12.5, 10.3.
MALDI-TOF: m/z = 5486 ($C_{344}H_{550}N_{14}Si_{14}Zn_3$, M^+ requires 5467).
λ_{max} ($CHCl_3$) / nm (log ε): 453 (5.64), 491 (5.35), 579 (4.48), 663 (4.60), 722 (5.17).

Cross pentamer synthesis: Due to solubility and stability issues, fully deprotected compounds ***x*Et-P1a** and ***x*-P1a** from **(TIPS)$_4$*x*Et-P1** and **(TMS)$_4$*x*-P1** were not isolated but directly engaged in reaction after a short silica plug (see text below).

Preparation of Cross Pentamer *x*Et-P5

To a solution of **(TIPS)$_4$*x*Et-P1** (26 mg, 20 μmol) in CH_2Cl_2 (4 mL) and pyridine (0.1 mL) was added TBAF (0.2 mL, 1.0 M solution in THF, 0.2 mmol). The solution was stirred at room temperature for 1 h and subsequently passed through a short silica plug (100:1 CH_2Cl_2:pyridine). The solution was not concentrated but directly added to a solution of mono-deprotected monomer (459 mg, 0.24 mmol) in CH_2Cl_2. The total solvent volume was adjusted to 25 mL by addition of CH_2Cl_2. Then, dry DIPA (5 mL), $Pd(PPh_3)_2Cl_2$ (18 mg, 26 μmol), CuI (25 mg, 0.13 mmol) and 1,4-benzoquinone (56 mg, 0.52 mmol) were added and the reaction mixture was stirred at room temperature for 3 h. The solution was then passed through a short silica plug (100:1 CH_2Cl_2:pyridine). The crude product was purified by column chromatography (3:1 40–60 petrol ether:CH_2Cl_2 + 1% pyridine) and size-exclusion chromatography (BioBeads SX-1, toluene) before precipitated using CH_2Cl_2/MeOH to yield ***x*Et-P5** (124 mg, 75%) as a brown solid.

^{1}H NMR (500 MHz, $CDCl_3$ + 1% pyridine-d5, 298 K): δ_H (ppm) 9.80 (d, J = 4.5 Hz, 8H), 9.66 (d, J = 4.5 Hz, 8H), 8.94 (d, J = 4.5 Hz, 8H), 8.88 (d, J = 4.4 Hz, 8H), 8.27 (s, 16H), 8.03 (s, 8H), 4.50–4.23 (m, 16H), 2.59 (t, J = 6.8 Hz, 8H), 2.28–2.20 (m, 8H), 2.13 (t, J = 7.2 Hz, 24H), 1.59–1.50 (m, 96H), 1.51–1.39 (m, 144H), 1.39–1.29 (m, 192H), 1.23–1.18 (m, 16H), 1.01–0.94 (m, 96H), 0.94–0.87 (m, 144H).
^{13}C NMR (125 MHz, $CDCl_3$+ 1% pyridine-d5, 298 K): δ_C (ppm) 152.8, 152.4, 150.8, 150.5, 148.4, 146.2, 140.8, 140.4, 139.3, 134.9, 133.3, 133.0, 130.8, 130.6, 124.6, 119.9, 111.1, 101.1, 100.1, 100.0,

96.7, 96.5, 94.9, 87.0, 82.5, 33.7, 31.8, 24.2, 22.8, 21.9 (broad), 21.8, 21.2, 18.8, 18.5, 17.3, 14.3, 12.9, 12.5, 10.4.
MALDI-TOF: *m/z* = 8231 ($C_{516}H_{800}N_{24}Si_{20}Zn_5$, M^+ requires 8214).
λ_{max} ($CHCl_3$) / nm (log ε): 441 (5.93), 550 (5.31), 667 (5.51), 818 (5.32).

Preparation of Cross Pentamer *x*-P5

To a solution of **(TMS)$_4$*x*-P1** (17 mg, 16 μmol) in CH_2Cl_2 (4 mL) and pyridine (0.1 mL) was added TBAF (0.2 mL, 1.0 M solution in THF, 0.2 mmol). The solution was stirred at room temperature for 1 h and subsequently passed through a short silica plug (100:1 CH_2Cl_2:pyridine). The solution was not concentrated but directly added to a solution of mono-deprotected monomer (360 mg, 0.19 mmol) in CH_2Cl_2. The total solvent volume was adjusted to 10 mL by addition of CH_2Cl_2. Then, dry DIPA (2 mL), $Pd(PPh_3)_2Cl_2$ (3.6 mg, 5.1 μmol), CuI (1.2 mg, 6.4 μmol) and 1,4-benzoquinone (2.8 mg, 26 μmol) were added and the reaction mixture was stirred at room temperature for 2 h. The solution was then passed through a short silica plug (3:1 40–60 petrol ether:CH_2Cl_2 + 1% pyridine), purified by size-exclusion chromatography (BioBeads SX-1, toluene) before precipitated using CH_2Cl_2/MeOH to yield ***x*-P5** (19 mg, 15%) as a brown solid.

^{1}H NMR (400 MHz, $CDCl_3$, 298 K): δ_H (ppm) 10.05 (s, 8H), 10.03 (d, J = 4.6 Hz, 8H), 9.73 (d, J = 4.6 Hz, 8H), 9.05 (d, J = 4.6 Hz, 8H), 8.97 (d, J = 4.6 Hz, 8H), 8.31 (s, 16H), 8.01 (s, 8H), 2.57 (t, J = 6.8 Hz, 8H), 2.27–2.18 (m, 8H), 1.55–1.47 (m, 96H), 1.43–1.35 (m, 144H), 1.34–1.24 (m, 192H) 1.23–1.16 (m, 16H), 0.98–0.91 (m, 96H), 0.91–0.83 (t, J = 7.0 Hz, 144H).
^{13}C NMR (100 MHz, $CDCl_3$, 298 K): δ_C (ppm) 153.3, 152.4, 151.0, 150.7, 140.6, 140.2, 139.5, 135.3, 133.8, 133.4, 132.7, 131.2, 124.8, 119.8, 111.1, 110.1, 103.4, 102.0, 99.9, 97.6, 88.2, 86.4, 83.5, 82.3, 65.2, 33.7, 31.8, 24.2, 22.8, 21.8, 21.2, 18.8, 18.5, 14.3, 12.8, 12.4, 10.3.
MALDI-TOF: *m/z* = 7941 ($C_{500}H_{768}N_{24}Si_{20}Zn_5$, M^+ requires 7989).
λ_{max} ($CHCl_3$) / nm (log ε): 438 (5.86), 518 (5.50), 582 (4.89), 635 (5.36), 742 (5.35).

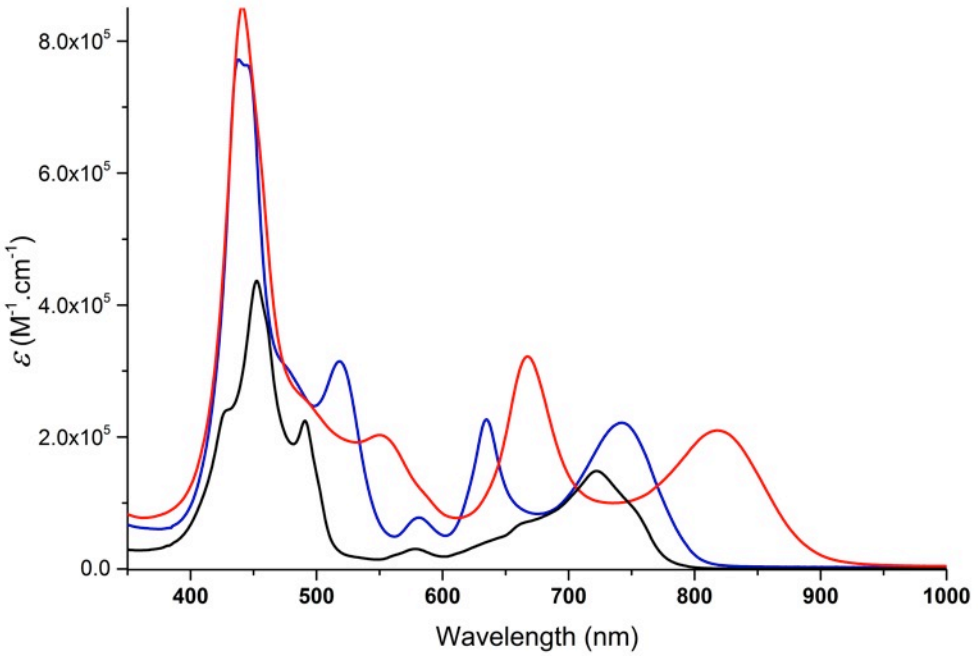

Figure S1. Extinction coefficient (ε) spectra of ***l*-P3$_{THS}$** (black), ***x*-P5** (blue) and ***x*Et-P5** (red) in $CHCl_3$ solution (298 K).

Preparation of *s*Et-P11·(T6)$_2$

Full deprotection of trimer ***l*-P3$_{THS}$** (28 mg, 5.1 μmol) was carried out in CH_2Cl_2 (10 mL) using TBAF (0.3 mmol, 0.3 mL, 1.0 M solution in THF). Full deprotection of cross pentamer ***x*Et-P5** (7.0 mg, 0.85 μmol) was realized following the same procedure, in CH_2Cl_2 (5 mL) using TBAF (50 μmol, 0.05 mL, 1.0 M solution in THF). Both crude mixtures were passed through a short silica plug ($CHCl_3$), mixed together and concentrated to 4 mL. Then, hexadentate template **T6** (3.4 mg, 3.4 μmol) was added and the resulting mixture was sonicated for 0.5 h. A catalyst solution was prepared by dissolving $Pd(PPh_3)_2Cl_2$ (0.5 mg, 0.7 μmol), CuI (0.7 mg, 3.4 μmol) and 1,4-benzoquinone (1.4 mg, 13 μmol) in dry $CHCl_3$ (1 mL) and freshly distilled DIPA (1 mL). This solution was added to the reaction mixture, which was stirred vigorously at room temperature for 2 h. The crude reaction solution was first passed through a plug of silica using (1:1 40–60 petrol ether:CH_2Cl_2), then over a size exclusion column on Biobeads SX-1 (toluene, 1% pyridine) and finally through recycling GPC (toluene, 1% pyridine). Fraction contained the desired product was further purified by column chromatography (95:5 40–60 petrol ether: CH_2Cl_2 + 1% pyridine) before precipitated using CH_2Cl_2/MeOH to yield ***s*Et-P11·(T6)$_2$** as a brown solid (3.8 mg, 23%).

^{1}H NMR (500 MHz, $CDCl_3$, 298 K): δ_H (ppm) 9.56 (d, J = 4.6 Hz, 8H), 9.55–9.49 (m, 24H), 9.44 (d, J = 4.5 Hz, 8H), 8.77–8.68 (m, 40H), 8.35–8.24 (m, 20H), 8.03–7.94 (m, 40H), 5.75 (d, J = 8.4 Hz, 4H), 5.67 (d, J = 9.1 Hz, 4H) , 5.61 (d, J = 7.2 Hz, 8H), 5.57 (d, J = 8.4 Hz, 8H), 5.53 (d, J = 7.4 Hz, 8H), 5.48–5.40 (m, 16H), 5.09 (d, J = 6.0 Hz, 10H), 4.99 (d, J = 6.7 Hz, 4H), 4.96 (d, J = 5.7 Hz, 8H), 4.45 (br s, 8H), 4.39–4.33 (m, 4H), 3.94 (br s, 8H), 2.41–2.37 (m, 10H), 2.36 (d, J = 6.7 Hz, 10H), 1.93 (br t, J = 6.7 Hz, 24H), 1.54–1.42 (m, 240H), 1.41–1.19 (m, 720H), 0.98–0.76 (m, 600H).
MALDI-TOF: *m/z* = 19702 (***s*Et-P11·(T6)$_2$**, $C_{1268}H_{1836}N_{56}Si_{40}Zn_{11}$, M^+ requires 19672).
λ_{max} ($CHCl_3$) / nm (log ε): 438 (5.67), 486 (5.91), 729 (5.36), 797 (5.59), 837 (5.78), 880 (5.82), 971 (4.71).

Preparation of *s*-P11·(T6)$_2$

Full deprotection of trimer ***l*-P3$_{THS}$** (33 mg, 6.0 μmol) was carried out in CH_2Cl_2 (10 mL) using TBAF (0.36 mmol, 0.36 mL, 1.0 M solution in THF). Full deprotection of cross pentamer ***x*-P5** (8 mg, 1.0 μmol) was realized following the same procedure, in CH_2Cl_2 (5 mL) using TBAF (60 μmol, 0.06 mL, 1.0 M solution in THF). Both crude mixtures were passed through a short silica plug ($CHCl_3$), mixed together and concentrated to 4 mL. Then, hexadentate template **T6** (4.0 mg, 4.0 μmol) was added and the resulting mixture was sonicated for 0.5 h. A catalyst solution was prepared by dissolving $Pd(PPh_3)_2Cl_2$ (0.6 mg, 0.8 μmol), CuI (0.8 mg, 4.0 μmol) and 1,4-benzoquinone (1.7 mg, 16 μmol) in dry $CHCl_3$ (1 mL) and freshly distilled DIPA (1 mL). This solution was added to the reaction mixture, which was stirred vigorously at room temperature for 2 h. The crude reaction solution was first passed through a plug of silica using (1:1 40–60 petrol ether:CH_2Cl_2), then over a size exclusion column on Biobeads SX-1 (toluene, 1% pyridine) and finally through recycling recycling GPC (toluene, 1% pyridine). Fraction contained the desired product was further purified by column chromatography (95:5 40–60 petrol ether: CH_2Cl_2 + 1% pyridine) before precipitated using CH_2Cl_2/MeOH to yield ***s*-P11·(T6)$_2$** as a brown solid (2.5 mg, 15%).

^{1}H NMR (500 MHz, $CDCl_3$, 298 K): δ_H (ppm) 9.58 (d, J = 4.5 Hz, 8H), 9.57 (d, J = 4.5 Hz, 8H), 9.55–9.51 (m, 24H), 9.30 (s, 8H), 8.80 (d, J = 4.6 Hz, 8H), 8.75 (d, J = 4.5 Hz, 8.73–8.68 (m, 24H), 8.33–8.26 (m, 20H), 8.08 (bs, 8H), 8.03–7.93 (m, 32H), 5.58–5.50 (m, 24H), 5.50–5.46 (m, 12H), 5.46–5.39

(m, 12H), 5.03 (bd, J = 6.1 Hz, 8H) , 4.98 (d, J = 6.2 Hz, 12H), 4.94 (d, J = 6.8 Hz, 4H), 2.74–2.65 (m, 4H), 2.45–2.35 (m, 20H), 1.54–1.18 (m, 960H), 1.00–0.84 (m, 456H), 0.83–0.76 (m, 144H).
MALDI-TOF: *m/z* = 19486 (***s*-P11·(T6)$_2$**, $C_{1252}H_{1804}N_{56}Si_{40}Zn_{11}$, M^+ requires 19449); *m/z* = 18485 (***s*-P11·T6**, $C_{1180}H_{1756}N_{50}Si_{40}Zn_{11}$, M^+ requires 18452); *m/z* = 17481 (***s*-P11**, $C_{1108}H_{1708}N_{44}Si_{40}Zn_{11}$, M^+ requires 17456).
λ_{max} ($CHCl_3$) / nm (log ε): 486 (5.84), 783 (5.58), 822 (5.78), 868 (5.87), 950 (4.52).

The synthesis of linear trimer having a central free-base porphyrin, ***l*-P3$_{ZnH2Zn}$**, is summarized in Scheme S2. ***l*-P3$_{ZnH2Zn}$** was synthesized using a statistical palladium-catalyzed reaction between the fully deprotected free-base monomer **P1a$_{2H}$** and a large excess of mono-deprotected zinc porphyrin monomer **P1a$_{Zn}$** in 39% yield.

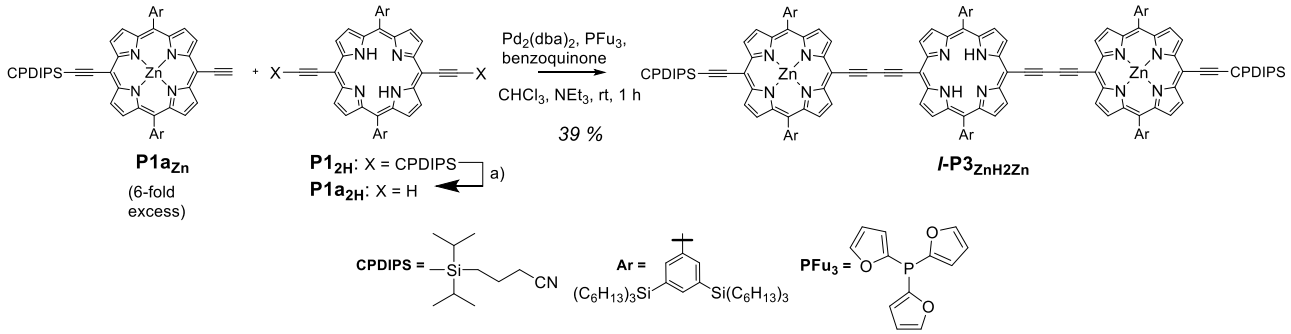

Scheme S2. Syntheses of linear trimer ***l*-P3$_{ZnH2Zn}$**. Conditions and reagents for a): TBAF, CH_2Cl_2, 20 °C. CPDIPS = cyanopropyldiisopropylsilyl. Ar = 3,5-bis(trihexylsilyl)phenyl.

Preparation of P1$_{2H}$

P1 (74 mg, 0.04 mmol) was dissolved in $CHCl_3$ (10 mL). Trifluoroacetic acid (0.1 mL) was added dropwise to the porphyrin solution and the reaction mixture was stirred at room temperature for 15 minutes. After completion of the reaction followed by TLC, pyridine was added (0.5 mL). The reaction mixture was immediately passed through a short plug of silica gel ($CHCl_3$) and concentrated to dryness to give the title compound as a dark solid (69 mg, 95%).

^{1}H NMR (500 MHz, $CDCl_3$, 298 K): δ_H (ppm) 9.61 (d, J = 4.6 Hz, 4H), 8.83 (d, J = 4.4 Hz, 4H), 8.24 (s, 4H), 8.02 (s, 2H), 2.56 (t, J = 6.8 Hz, 4H), 2.25–2.16 (m, 4 H), 1.54–1.47 (m, 24H), 1.43–1.36 (m, 24H), 1.36–1.26 (m, 48H), 0.99–0.92 (m, 24H), 0.89 (t, J = 6.3 Hz, 36H), –2.10 (s, 2H).
^{13}C NMR (125 MHz, $CDCl_3$, 298 K): δ_C (ppm) 140.3, 139.6, 139.5, 135.4, 123.4, 119.8, 109.6, 100.5, 9.9, 33.6, 31.7, 24.2, 22.8, 1.7, 21.2, 18.7, 18.5, 14.3, 12.8, 12.4, 10.2.
MALDI-TOF: *m/z* = 2006.4 ($C_{128}H_{212}N_6Si_6$, M^+ requires 2002.5).
λ_{max} ($CHCl_3$) / nm log(ε): 680 (4.4), 620 (3.8), 585 (4.7), 544 (4.1), 443 (5.4), 433 (5.5).

Preparation of P1a$_{2H}$

P1$_{2H}$ (69 mg, 0.03 mmol) was dissolved in CH_2Cl_2 (5 mL) under nitrogen. TBAF solution (1.0 M in THF) (0.1 mL, 0.1 mmol) was added dropwise to the reaction mixture which was stirred at room temperature for 15 minutes. Then acetic acid (50 μL) was added and the crude reaction mixture was immediately passed though a short plug of silica gel ($CHCl_3$). Fraction contained the desired product was concentrated to dryness and used in the next step without further purification (61 mg, 99%).

^{1}H NMR (400 MHz, $CDCl_3$, 298 K): δ_H (ppm) 9.66 (d, J = 4.7 Hz, 4H), 8.86 (d, J = 4.5 Hz, 4H), 8.27 (s, 4H), 8.01 (s, 2H), 4.21 (s, 2H), 1.54–1.44 (m, 24H), 1.43–1.27 (m, 72H), 0.99–0.92 (m, 24H), 0.89 (t, J = 7.0 Hz, 36H), –2.24 (s, 2H).

Preparation of *l*-P3$_{ZnH2Zn}$

P1a$_{2H}$ (61.0 mg, 37.0 μmol), mono-deprotected monomer **P1** (480 mg, 0.26 mmol), $Pd_2(dba)_3$ (17.0 mg, 18.5 μmol), tri-2-furylphosphine (34.4 mg, 0.15 mmol) and 1,4-benzoquinone (48.0 mg, 0.44 mmol) were dissolved in a mixture of toluene and triethylamine (5:1) (20 mL). The reaction mixture was stirred at 60 ˚C for 24 h. The solvents were removed and the mixture was purified over a plug of silica gel ($CHCl_3$ + 1% pyridine). Fraction contained the desired product was further purified by SEC column ($CHCl_3$ + 1% pyridine) and concentrated to dryness to yield ***l*-P3$_{ZnH2Zn}$** as a dark green solid (78.0 mg, 39%).

^{1}H NMR (500 MHz, $CDCl_3$ + 1% pyridine-d5, 298 K): δ_H (ppm) 9.94 (d, J = 4.6 Hz, 4H), 9.89 (d, J = 4.7 Hz, 4H), 9.70 (d, J = 4.5 Hz, 4H), 9.00 (d, J = 4.6 Hz, 4H), 8.95 (d, J = 4.7 Hz, 4H), 8.93 (d, J = 4.5 Hz, 4H), 8.38 (s, 4H), 8.31 (s, 8H), 8.08 (s, 2H), 8.05 (s, 4H), 2.59 (t, J = 6.9 Hz, 4H), 2.29–2.20 (m, 4H), 1.60–1.50 (m, 72H), 1.50–1.39 (m, 96H), 1.39–1.30 (m, 144H), 1.24–1.18 (m, 8H), 1.04–0.95 (m, 72H), 0.95–0.87 (m,108H), –1.50 (s, 2H).
^{13}C NMR (125 MHz, $CDCl_3$+ 1% pyridine-d5, 298 K): δ_C (ppm) 152.3, 150.9, 150.6, 143.5, 140.9, 140.6, 139.7, 139.5, 139.4, 136.2, 135.6, 135.1, 133.5, 133.2, 131.0, 130.9, 124.7, 124.2, 122.6, 119.9, 99.6, 96.9, 88.9, 86.9, 83.6, 82.2, 33.7, 31.8, 24.2, 22.9, 21.8, 21.2, 18.8, 18.5, 14.3, 12.8, 10.0.
MALDI-TOF: m/z = 5417 ($C_{344}H_{552}N_{14}Si_{14}Zn_2$, M^+ requires 5406).
λ_{max} ($CHCl_3$) / nm log(ε): 751 (5.1), 659 (4.9), 598 (4.4), 455 (5.7).

C. Characterization of Spiro-Nanoring-Template Complexes (spectra & analysis)

C1. Characterization of ***s*-P11·(T6)$_2$**: *NMR analysis and Mass Spectra*

Based on the D_{2d} symmetry of ***s*-P11·(T6)$_2$** complex, only one quarter of the molecule needs to be considered in the interpretation of the ^{1}H NMR spectrum (Figure S2). The chemical structure in Figure S2 represents the four porphyrin units ($\mathbf{P_S}$ where s is for spiro, $\mathbf{P_A}$, $\mathbf{P_B}$ and $\mathbf{P_C}$) contained in this quarter and the portion of the template that coordinates the porphyrin units. The full assignment of the ^{1}H NMR spectrum for the ***s*-P11·(T6)$_2$** complex is outlined in the following section (Figure S2). This was completed by comparison with similar template-ring systems[S5] and with the assistance of COSY and NOESY NMR experiments.

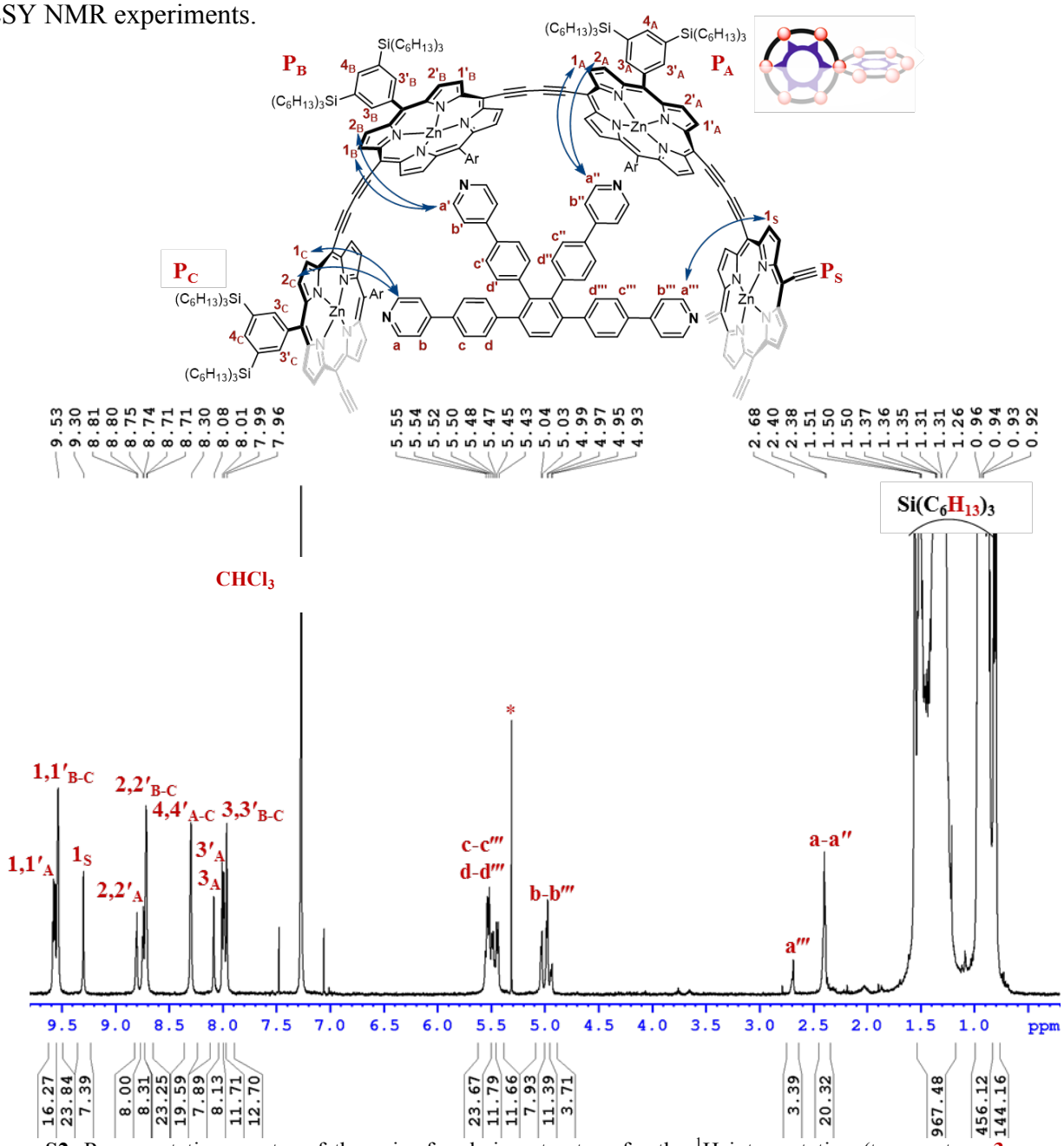

Figure S2. Representative quarter of the spiro-fused ring structure for the ^{1}H interpretation (top, protons $\mathbf{3_{A\text{-}C}}$ are pointing to the inside of the ring (towards the template) and protons $\mathbf{3'_{A\text{-}C}}$ to the outside of the ring, arrows for keys NOEs) and ^{1}H NMR spectrum of ***s*-P11·(T6)$_2$** (bottom, 500 MHz, $CDCl_3$, 298 K,* for dichloromethane).

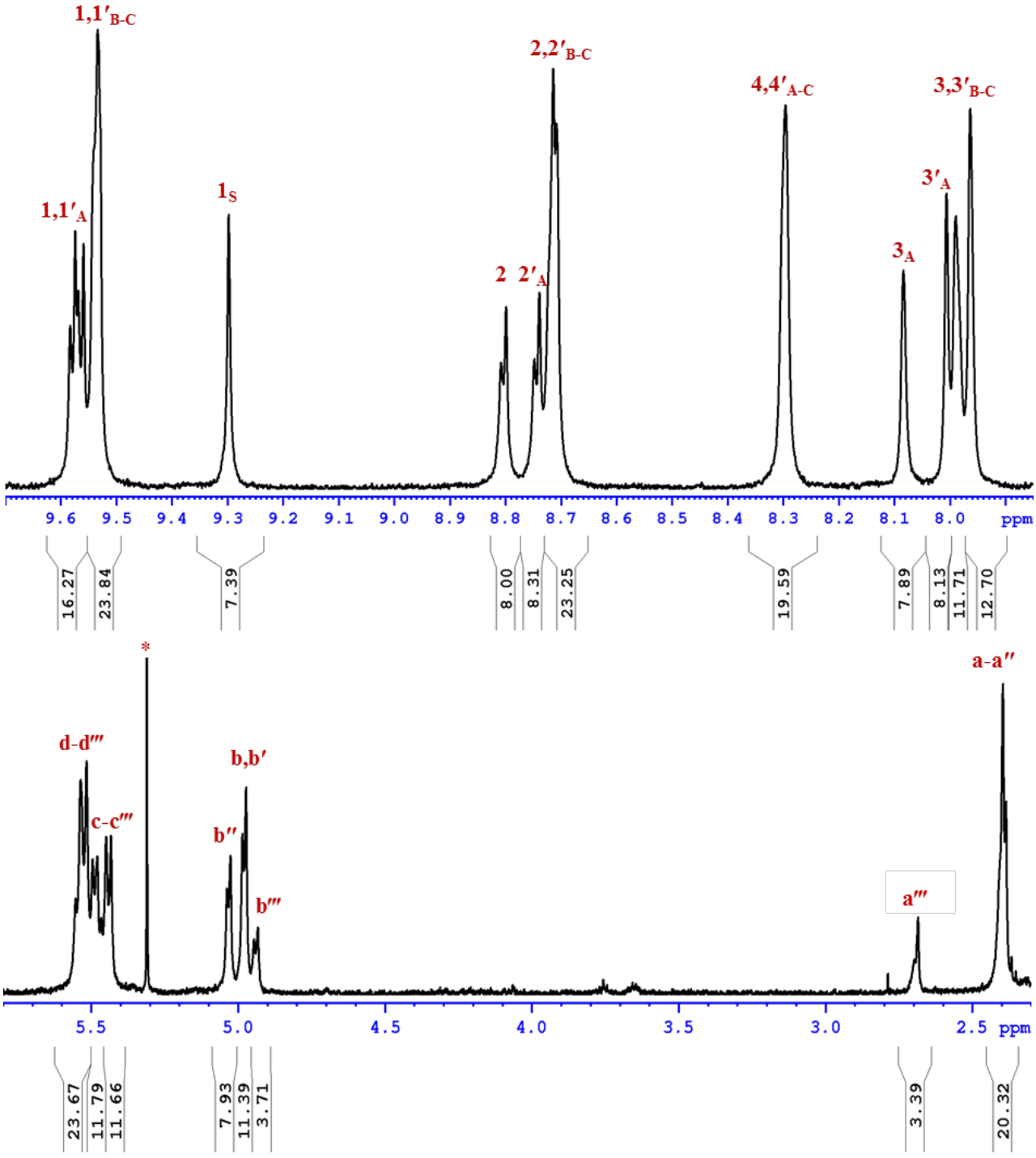

Figure S3. Expansions of the keys regions of the ^{1}H NMR spectrum of ***s*-P11·(T6)$_2$** (500 MHz, $CDCl_3$, 298 K, * for dichloromethane).

The proton assignments for ***s*-P11·(T6)$_2$** is based on the initial assumption that the porphyrin β-protons between 9.20 and 9.70 ppm, correspond to protons **1**$_{A\text{-}C}$, **1′**$_{A\text{-}C}$ and **1**$_S$ which are adjacent to the butadiyne bridge in ***s*-P11·(T6)$_2$**. This assumption was later confirmed by COSY and NOESY experiments.

Due to ring current effect, the α-protons **a**, **a′**, **a″** and **a‴** on the **T6** template pyridine moieties are strongly shielded and appear at very low chemical shifts (around 2.40 ppm for **a**, **a′** and **a″** and 2.70 ppm for **a‴**).

In the NOESY spectrum (Figure S4), the porphyrin β-protons **1**,**1′**$_A$ and **1**,**1′**$_{B\text{-}C}$ show NOE with the template α-protons **a**, **a′** and **a″** and the porphyrin β-protons **1**$_S$ show NOE with the template α-protons **a‴**. Additionally, the porphyrin β-protons **1**,**1′**$_A$ show NOE with protons **1**$_S$ of the spiro porphyrin **P**$_S$ which confirm that β-protons **1**,**1′**$_A$ belong to the four porphyrins **P**$_A$ directly bound to the spiro porphyrin.

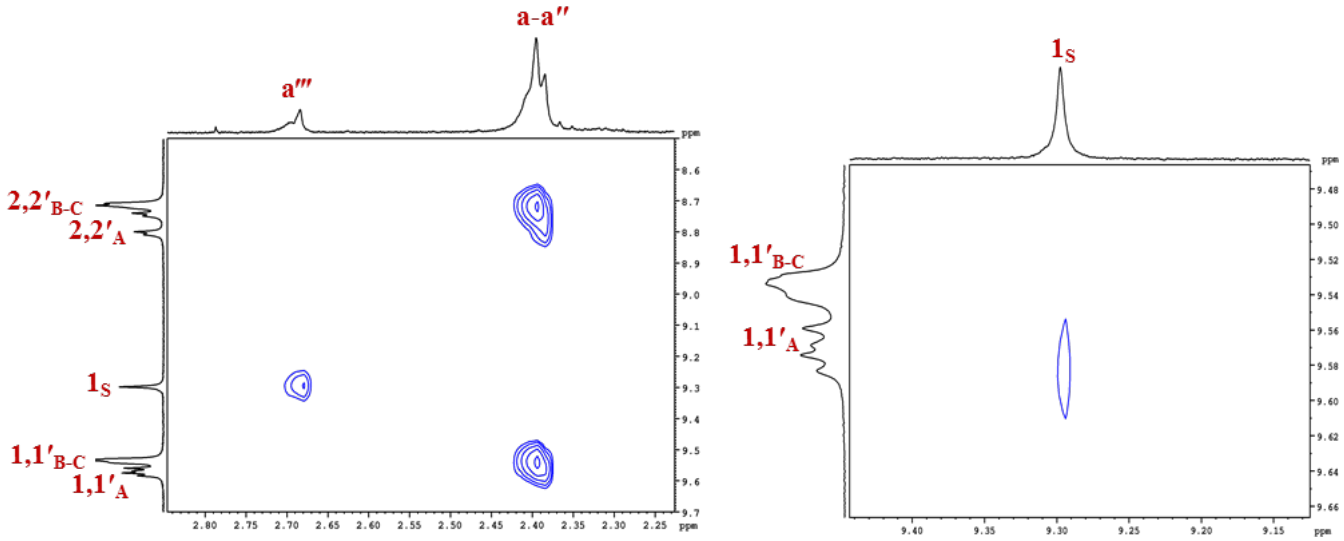

Figure S4. Regions of the NOESY spectrum of ***s*-P11·(T6)$_2$** corresponding to the porphyrin β-protons and the **T6** pyridine template α-protons (500 MHz, $CDCl_3$, 298 K).

The template β-protons **b**, **b′**, **b″** and **b‴** are less affected by the ring current and are therefore less shielded than α-protons **a**, **a′**, **a″** and **a‴**. Based on their coupling with protons **a**, **a′**, **a″** and **a‴** in the COSY spectrum, their assignment can be confirmed (Figure S5). Based on their integration and the symmetry of the molecule, template β-protons **b**, **b′**, **b″** can be readily assigned.

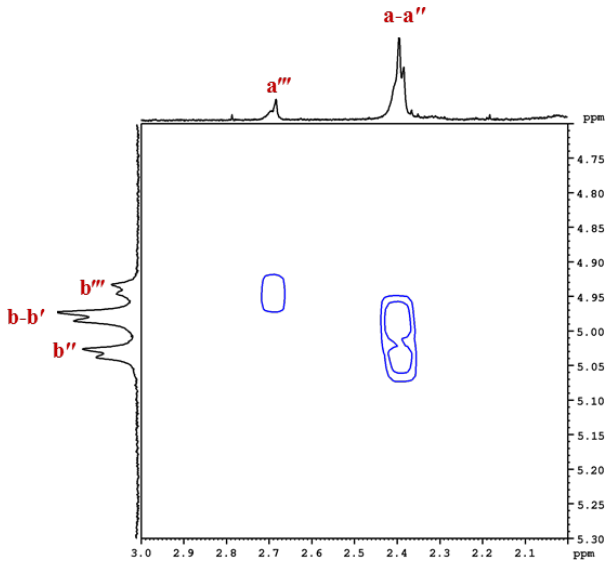

Figure S5. Region of the COSY spectrum of ***s*-P11·(T6)$_2$** corresponding to the **T6** pyridine template **α**- and **β**-protons (500 MHz, $CDCl_3$, 298 K).

In the NOESY spectrum, template protons **b**, **b′**, **b″** and **b‴** show NOEs with protons **c**, **c′**, **c″** and **c‴** respectively (Figure S6, left. The NOE between **b‴** and **c‴** was difficult to analyze because of the overlap of protons **c″** and **c‴**). This helps clarify the assignment for protons **d**, **d′**, **d″** and **d‴** that couple to protons **c**, **c′**, **c″** and **c‴**, respectively, in the COSY spectrum (Figure S6, right).

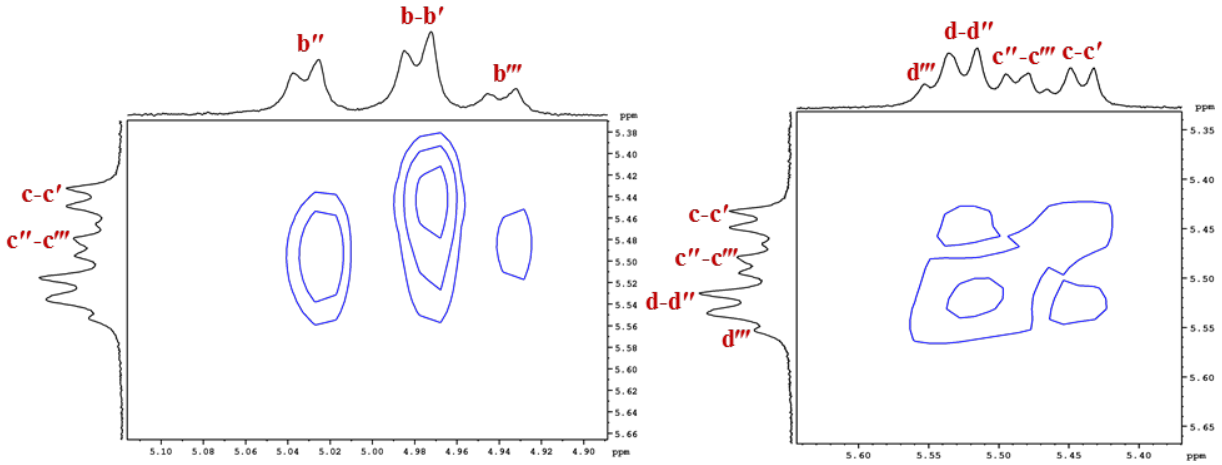

Figure S6. Regions of the NOESY (left) and COSY (right) spectrum of ***s*-P11·(T6)$_2$** corresponding to the **T6** pyridine template **β**-, **γ**- and **δ**-protons (500 MHz, $CDCl_3$, 298 K).

The porphyrin β-protons between 8.65 and 8.85 ppm correspond to protons **2,2′$_{A-C}$** based on their correlations with protons **1,1′$_{A-C}$** in the COSY spectrum (Figure S7, left). The protons of the aryl solubilizing side groups can also be assigned based on their correlations with protons **2,2′$_{A-C}$** in the NOESY spectrum (Figure S7, right).

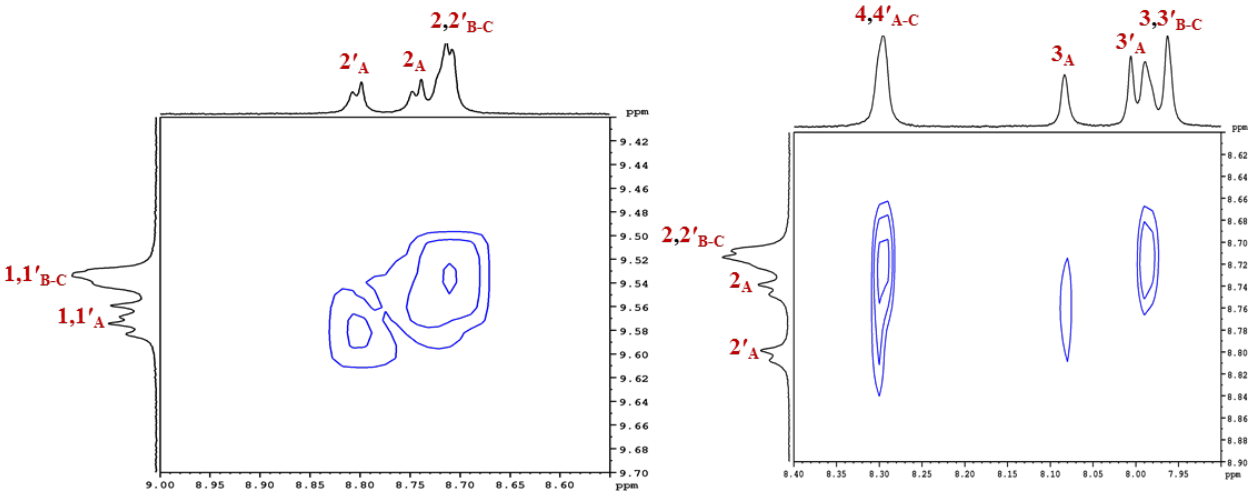

Figure S7. Regions of the COSY (left) and NOESY (right) spectrum of ***s*-P11·(T6)$_2$** corresponding to the porphyrin β- and aryl protons (500 MHz, $CDCl_3$, 298 K).

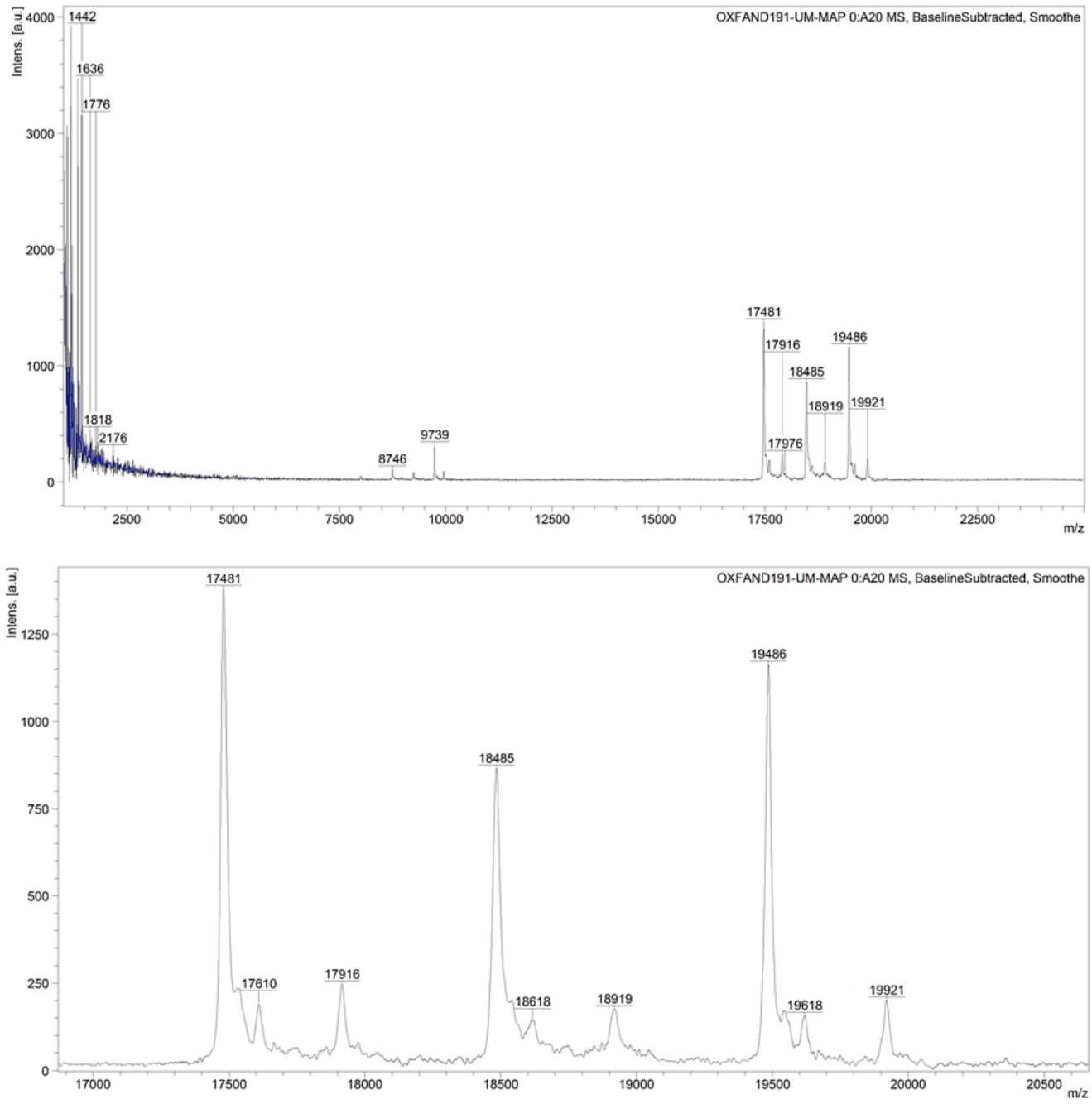

Figure S8. MALDI-MS spectrum of ***s*-P11·(T6)$_2$**, obtained from the EPSRC National Mass Spectrometry Facility, Swansea. The mass of the molecular ions matches well with that expected for ***s*-P11**: *m/z* = 19486 (***s*-P11·(T6)$_2$**, $C_{1252}H_{1804}N_{56}Si_{40}Zn_{11}$, M^+ requires 19449); *m/z* = 18485 (***s*-P11·(T6)**, $C_{1180}H_{1756}N_{50}Si_{40}Zn_{11}$, M^+ requires 18452); *m/z* = 17481 (***s*-P11**, $C_{1108}H_{1708}N_{44}Si_{40}Zn_{11}$, M^+ requires 17456).

C2. Characterization of ***s*Et-P11·(T6)$_2$**: *NMR analysis and Mass spectra*

The assignment of the relevant protons for the complex ***s*Et-P11·(T6)$_2$** (Figure S9–S10) was carried out by comparison with the complex ***s*-P11·(T6)$_2$** and with the assistance of 2D COSY and NOESY NMR experiments.

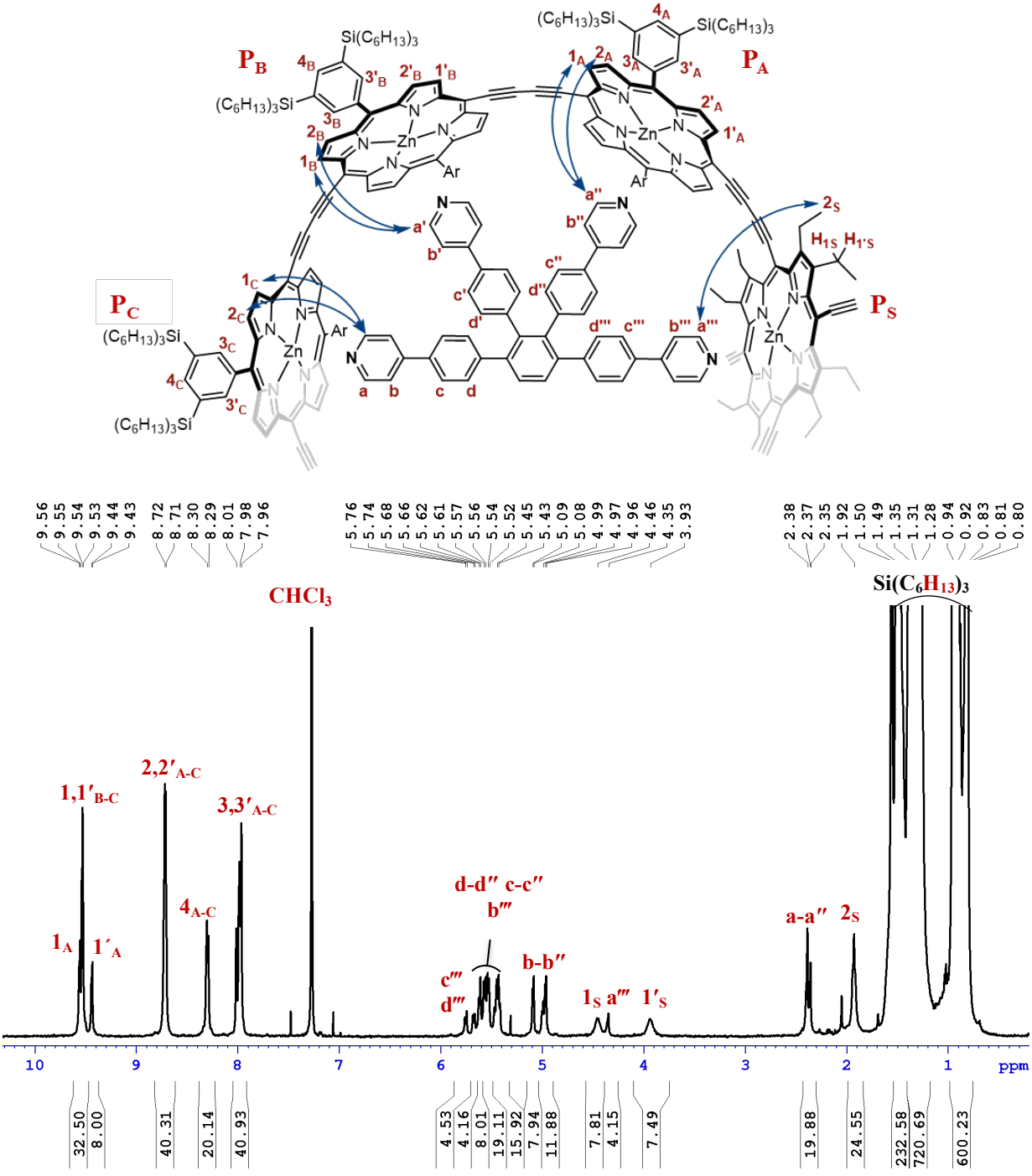

Figure S9. Representative quarter of the fused ring structure for the ^{1}H interpretation (top, protons **3$_{A-C}$** are pointing to the inside of the ring (towards the template) and protons **3′$_{A-C}$** to the outside of the ring, arrows for keys NOEs) and ^{1}H NMR spectrum of ***s*Et-P11· (T6)$_2$** (bottom, 700 MHz, $CDCl_3$, 298 K).

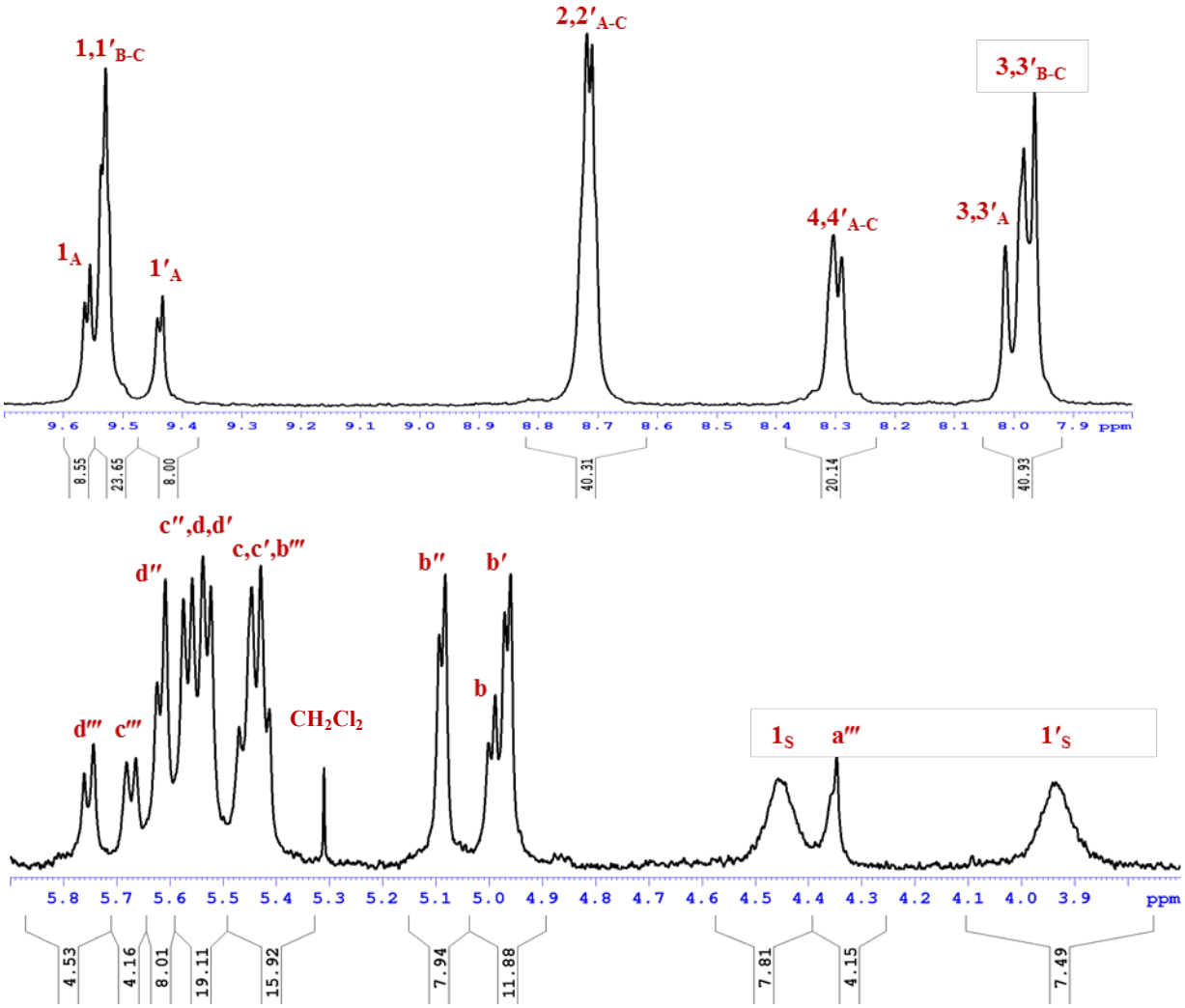

Figure S10. Expansions of the keys regions of the ^{1}H NMR spectrum of ***s*Et-P11·(T6)$_2$** (700 MHz, $CDCl_3$, 298 K).

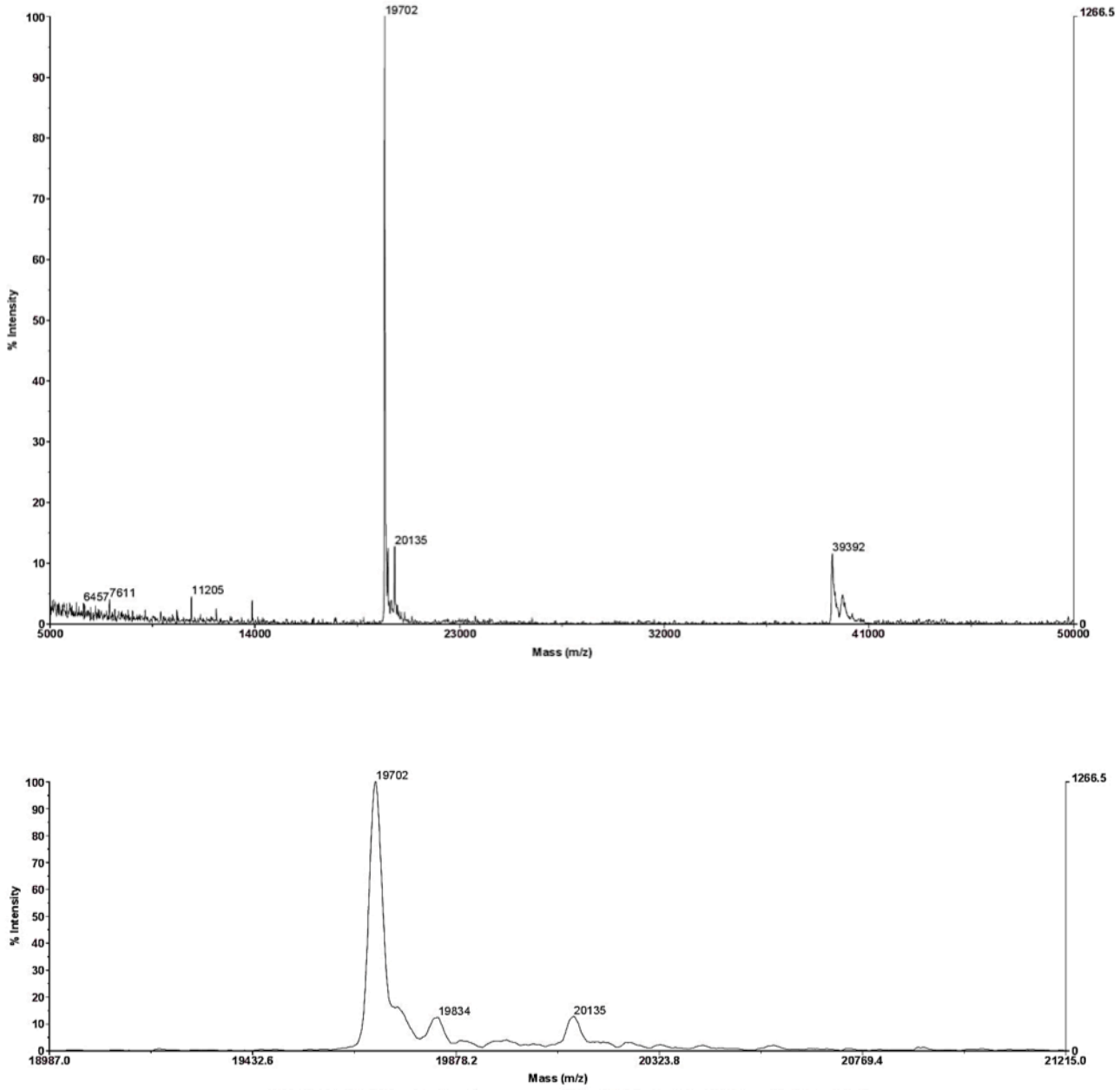

Figure S11. MALDI-MS spectrum of ***s*Et-P11·(T6)$_2$**, obtained from the EPSRC National Mass Spectrometry Facility, Swansea. The expected molecular ion [***s*Et-P11·(T6)$_2$**]$^+$ is the dominant signal: *m/z* = 19702 (***s*Et-P11·(T6)$_2$**, $C_{1268}H_{1836}N_{56}Si_{40}Zn_{11}$, M^+ requires 19673).

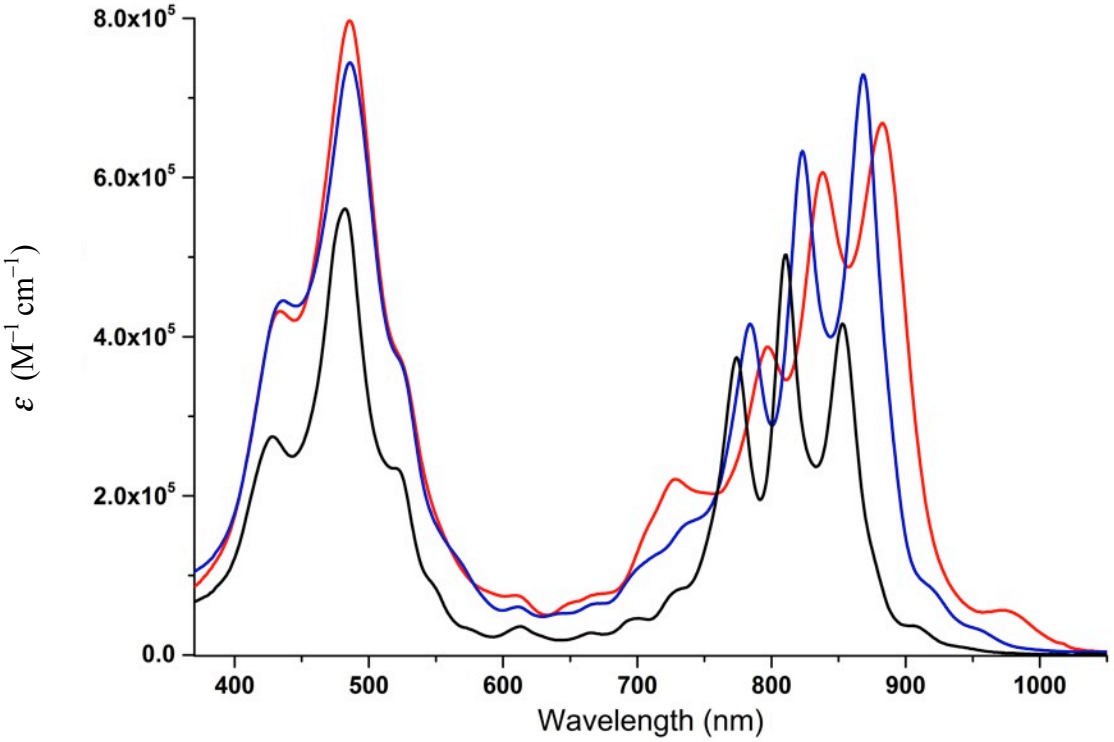

Figure S12. Extinction coefficient (ε) spectra of ***c*-P6·T6** (black), ***s*-P11·(T6)$_2$** (blue) and ***s*Et-P11·(T6)$_2$** (red) in toluene with 1% pyridine solution (298 K).

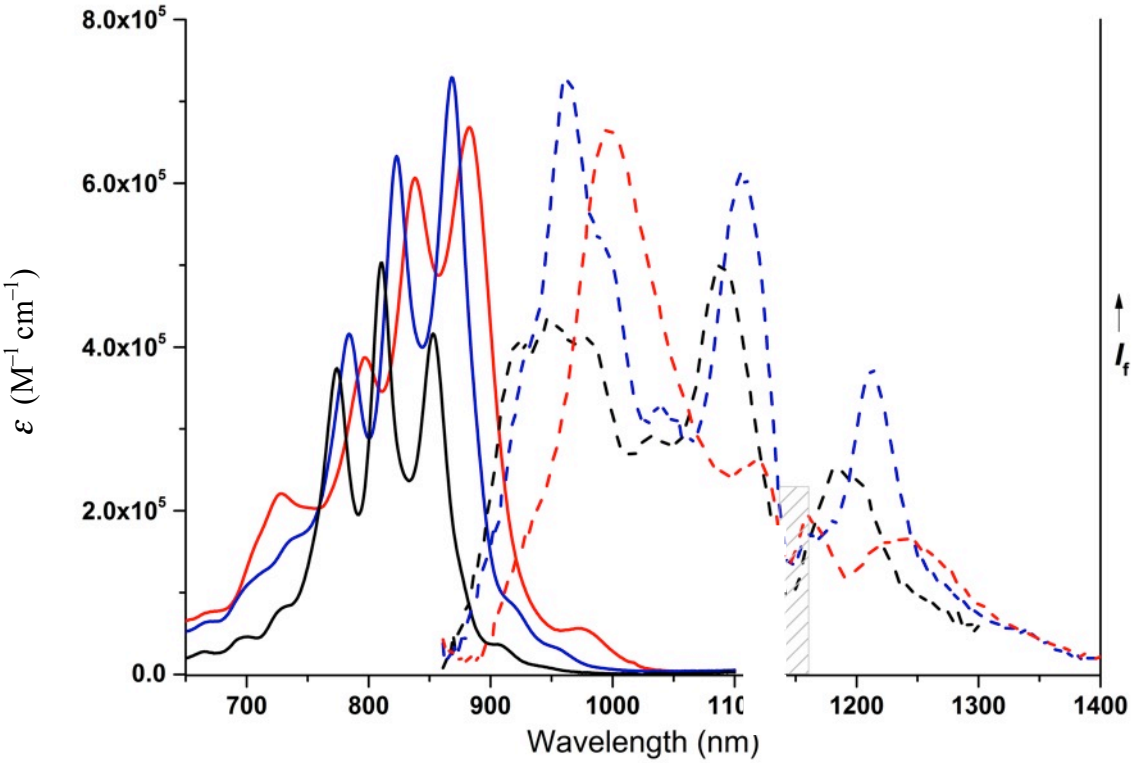

Figure S13. Partial extinction coefficient (ε, solid line) and normalized fluorescence spectra (dashed line) of ***c*-P6·T6** (black), ***s*-P11·(T6)$_2$** (blue) and ***s*Et-P11·(T6)$_2$** (red) in toluene with 1% pyridine solution (298 K). Data between 1130 and 1170 nm were omitted due to solvent absorption effect.

D. UV-Vis-NIR titrations

All titrations were performed in chloroform (containing ca. 0.5% ethanol as stabilizer) at 298 K and at constant porphyrin concentration (by adding porphyrin to the ligand stock solution before titrations were started). A key assumption underlying the analysis presented here is that each step in the titrations can be analyzed as an all-or-nothing two-state equilibrium. This assumption is supported by the isosbestic nature of the UV/vis titration for each step (Figure S14–25) and by the good fits to the calculated binding curves. Moreover, the measured binding constants are in good agreement with similar systems, previously reported.[S4,S6]

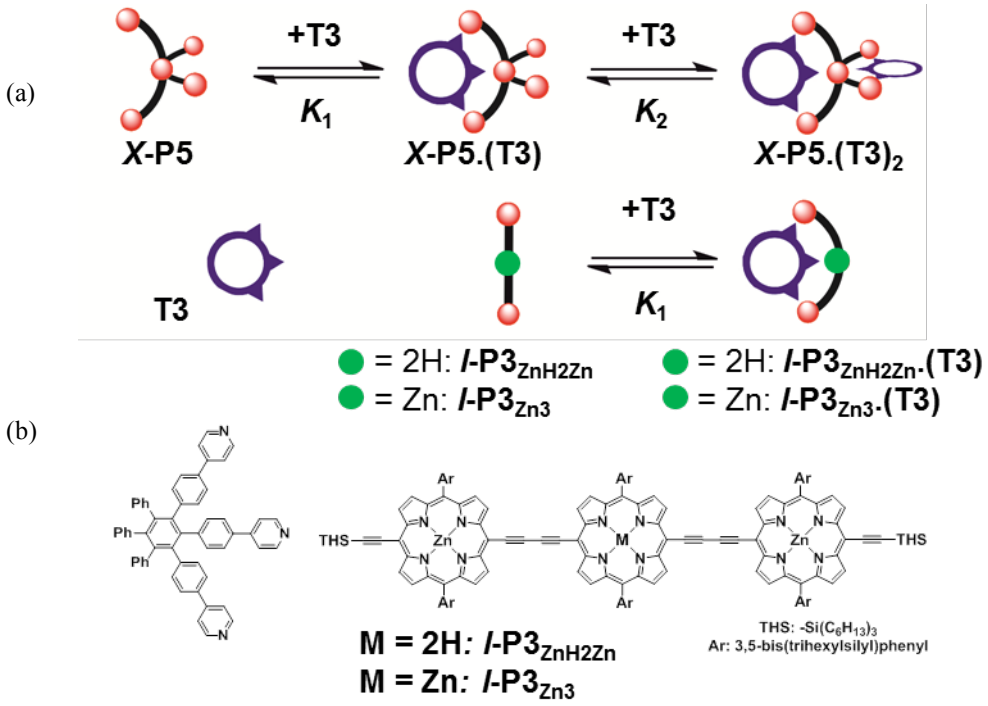

Figure S14. (a) Representation of the two-stage complexation of cross-pentamer ***x*-P5** with **T3** and the 1:1 complexation of linear trimers ***l*-P3$_{ZnH2Zn}$** and ***l*-P3$_{Zn3}$** with **T3**, and (b) the corresponding structures of the linear trimers and template **T3**.

D1. Determination of K_1 *values by titration of* ***x*Et-P5·(T3)**, ***x*-P5·(T3)** *and* ***l*-P3$_{Zn3}$** *with pyridine.*
Determination of K_1 was studied by break-up titration for complexes ***x*Et-P5·T3** and ***x*-P5·T3** with pyridine, because of the high binding constant for the formation of these complexes makes it difficult to determine their stabilities by direct titration. As a reference, complex ***l*-P3$_{Zn3}$·T3** was also studied under identical conditions.

The complexes ***x*Et-P5·T3**, ***x*-P5·T3** and ***l*-P3$_{Zn3}$·T3** were firstly prepared by adding one equivalent of **T3** to a solution of ***x*Et-P5**, ***x*-P5** or ***l*-P3$_{Zn3}$**. Then, a large excess of pyridine was titrated into solutions of the 1:1 complex (ca. 10^{-6} M in $CHCl_3$ at 298 K) to displace the multidentate ligand. The denaturation constant K_d was determined from this titration and used to calculate the formation constants K_1 *via* the corresponding thermodynamic cycle shown below (the same thermodynamic cycle can be drawn for ***x*Et-P5** and ***l*-P3$_{Zn3}$**).[S5]

$$K_1 = \frac{K_{py}^{\ 3}}{K_d}$$

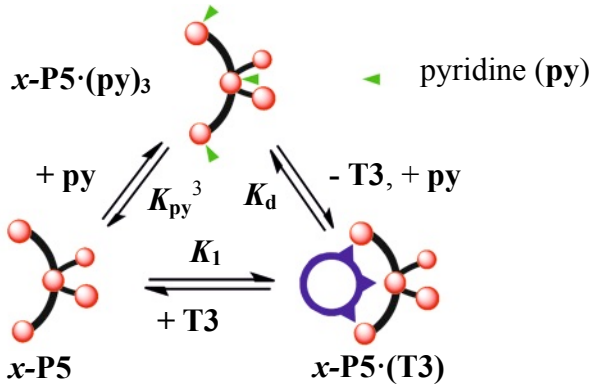

Figure S15. Thermodynamic cycle relating the formation constant of the template complex ***x*-P5·(T3)** (K_1) to the denaturation constant (K_d) and binding constant of each porphyrin unit for pyridine to form ***x*-P5·(py)$_3$** ($K_{py}^{\ 3}$). Note that pyridine will also bind to the other two sites on ***x*-P5**, but this process occurs in a different range of pyridine concentrations, so it can be ignored when analyzing the denaturation.

Where:

K_1 is the formation constant for the complex ***x*-P5·T3** (also ***x*Et-P5·T3** and ***l*-P3$_{Zn3}$·T3**) from the corresponding cross-pentamer (or trimer).

$K_{py}^{\ 3}$ is the cube of the binding constant for coordination of pyridine to zinc porphyrin monomer (K_{py} = 3280 M^{-1} under our conditions), measured as previously described.[S5,S6]

K_d is the denaturation constant determined by fitting the titration data using the Origin™ software;[S4] see K_d values, curves and spectra in Figure S16–S21.

The resulting values of K_1 are listed in Table S1. Statistical factors, K_σ,[S7-S9] were calculated as described below (Section D3), and used to calculate the statistically-corrected 1:1 association constants K_{chem} using the equation $K_{chem} = K_1 / K_\sigma$.

Table S1. Association constants of complexes ***x*Et-P5·T3**, ***x*-P5·T3** and ***l*-P3$_{Zn3}$·T3** measuring by break-up titration with pyridine (298 K, $CHCl_3$). Statistical factors are explained in Section D4.

		***x*-P5·T3**	***x*Et-P5·T3**	***l*-P3$_{Zn3}$·T3**
K_1	Run 1	$(3.0 \pm 0.3) \times 10^8$ M^{-1}	$(6.4 \pm 0.9) \times 10^{11}$ M^{-1}	$(1.2 \pm 0.2) \times 10^8$ M^{-1}
	Run 2	$(2.6 \pm 0.3) \times 10^8$ M^{-1}	$(5.3 \pm 0.9) \times 10^{11}$ M^{-1}	$(1.2 \pm 0.2) \times 10^8$ M^{-1}
	Average	$(2.8 \pm 0.4) \times 10^8$ M^{-1}	$(5.9 \pm 1.2) \times 10^{11}$ M^{-1}	$(1.2 \pm 0.2) \times 10^8$ M^{-1}
K_σ		32		16
K_{chem}		$(8.8 \pm 1.3) \times 10^6$ M^{-1}	$(1.8 \pm 0.4) \times 10^{10}$ M^{-1}	$(7.5 \pm 1.9) \times 10^6$ M^{-1}
spectra		Fig. S16–17	Fig. S18–19	Fig. S20–21

D1a. Break-up titration of ***x*-P5·T3** *with pyridine*

a) b)

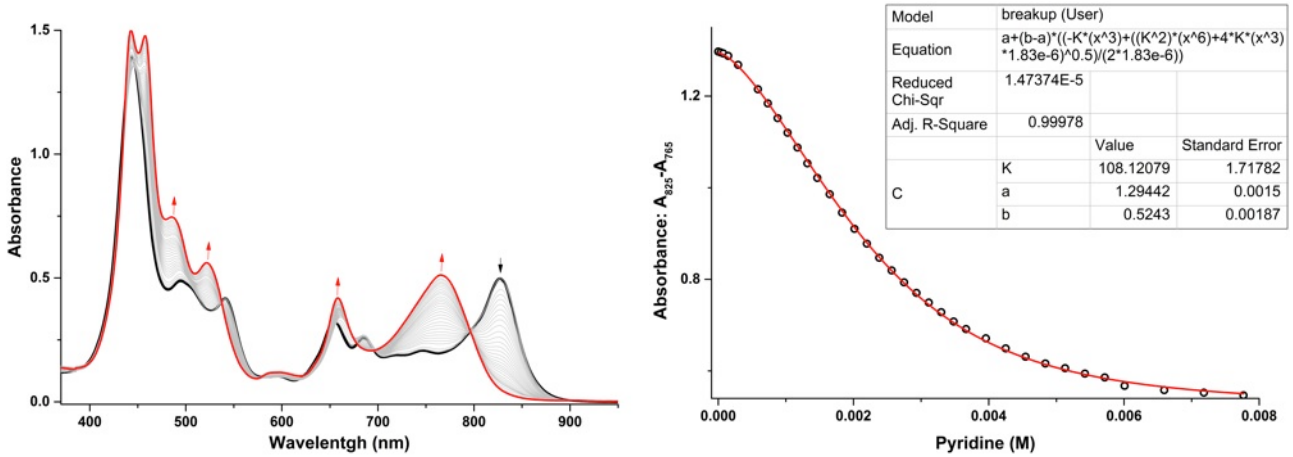

Figure S16. UV/vis/NIR break-up titration of ***x*-P5·T3** ([***x*-P5·T3**] = 1.8 × 10^{-6} M) with pyridine in $CHCl_3$ at 298 K. (a) Changes in absorption upon addition of pyridine. Arrows indicate areas of increasing (red) and decreasing (black) absorption during the titration; (b) Binding isotherm (black dots) derived from the difference of absorption data at λ = 825 and 765 nm and calculated fit (red line, from ORIGIN™ software). Run 1: $\boldsymbol{K}_\mathbf{d}$ = 108 ± 2 M^{-2}, R^2 = 0.999.

a) b)

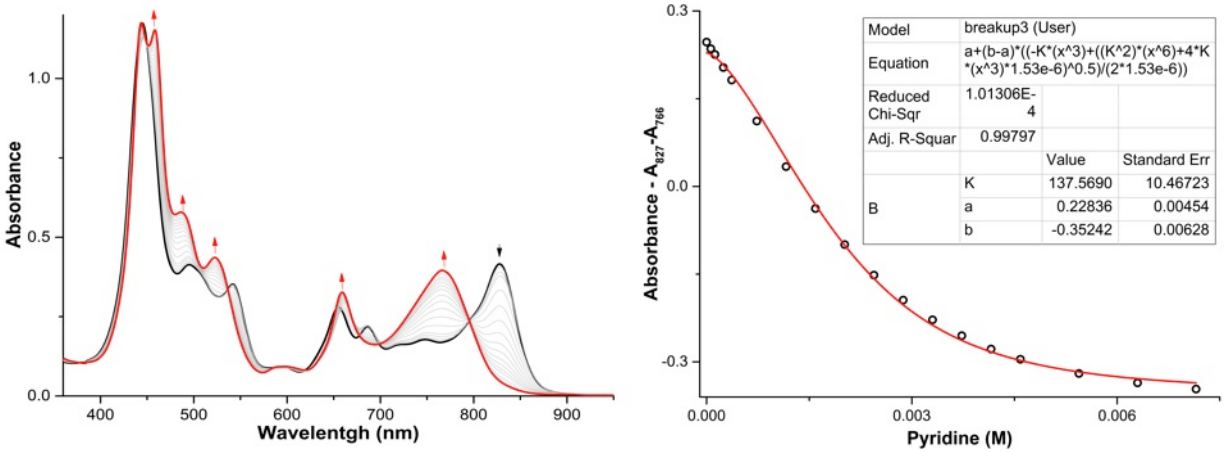

Figure S17. UV/vis/NIR break-up titration of ***x*-P5·T3** ([***x*-P5·T3**] = 1.5 × 10^{-6} M) with pyridine in $CHCl_3$ at 298 K. (a) Changes in absorption upon addition of pyridine. Arrows indicate areas of increasing (red) and decreasing (black) absorption during the titration; (b) Binding isotherm (black dots) derived from the difference of absorption data at λ = 827 and 766 nm and calculated fit (red line, from ORIGIN™ software). Run 2: $\boldsymbol{K}_\mathbf{d}$ = 137 ± 10 M^{-2}, R^2 = 0.998.

D1b. Break-up titration of ***x*Et-P5·T3** *with pyridine.*

a) b)

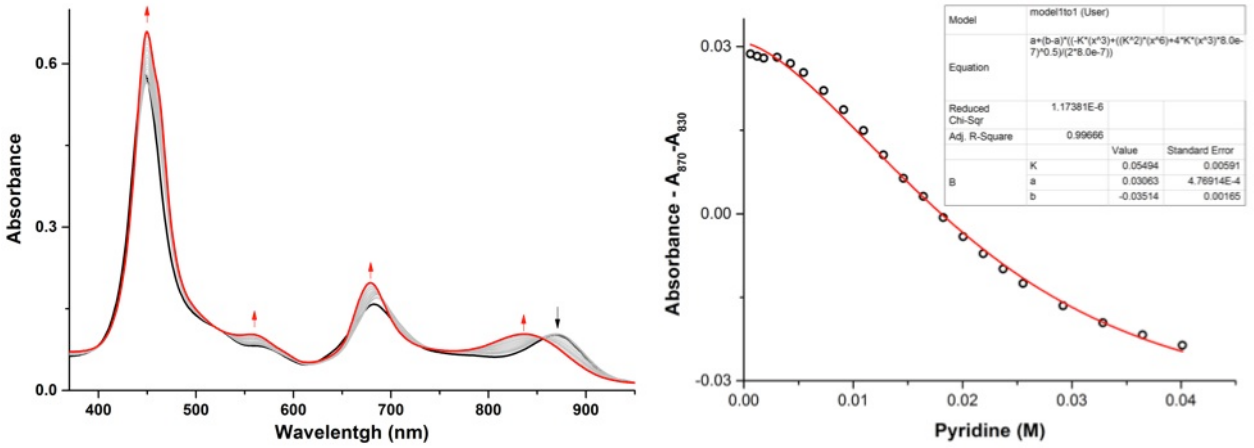

Figure S18. UV/vis/NIR break-up titration of ***x*Et-P5·T3** ([***x*Et-P5·T3**] = 8.0 × 10^{-7} M) with pyridine in $CHCl_3$ at 298 K. (a) Changes in absorption upon addition of pyridine. Arrows indicate areas of increasing (red) and decreasing (black) absorption during the titration; (b) Binding isotherm (black dots) derived from the difference of absorption data at λ = 870 and 830 nm and calculated fit (red line, from ORIGIN™ software). Run 1: $\boldsymbol{K_d}$ = 0.055 ± 0.006 M^{-2}, R^2 = 0.997.

a) b)

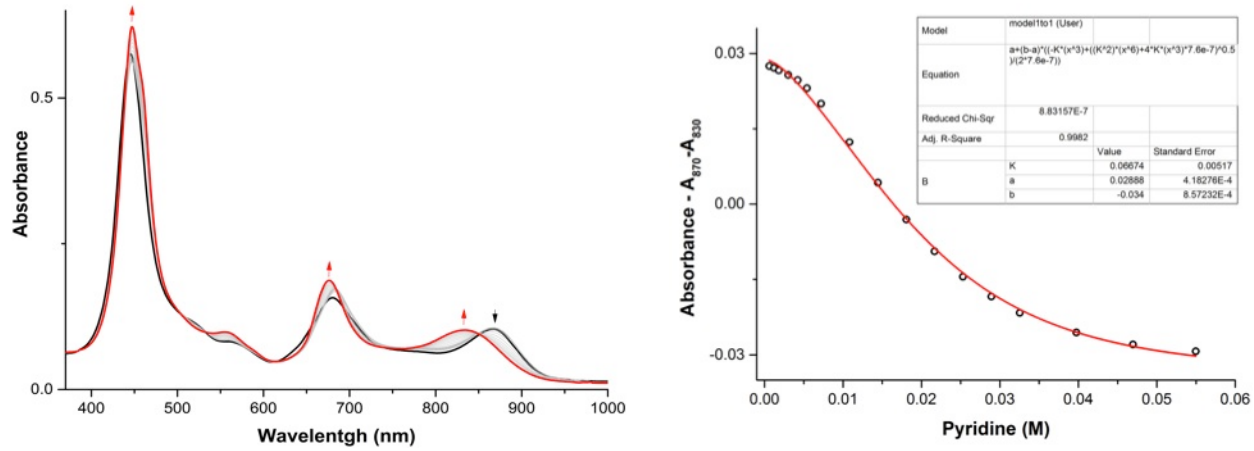

Figure S19. UV/vis/NIR break-up titration of ***x*Et-P5·T3** ([***x*Et-P5·T3**] = 7.6 × 10^{-7} M) with pyridine in $CHCl_3$ at 298 K. (a) Changes in absorption upon addition of pyridine. Arrows indicate areas of increasing (red) and decreasing (black) absorption during the titration; (b) Binding isotherm (black dots) derived from the difference of absorption data at λ = 870 and 830 nm and calculated fit (red line, from ORIGIN™ software). Run 2: $\boldsymbol{K_d}$ = 0.067 ± 0.005 M^{-2}, R^2 = 0.998.

D1c. Break-up titration of ***l*-P3$_{Zn3}$·T3** *with pyridine.*

a) b)

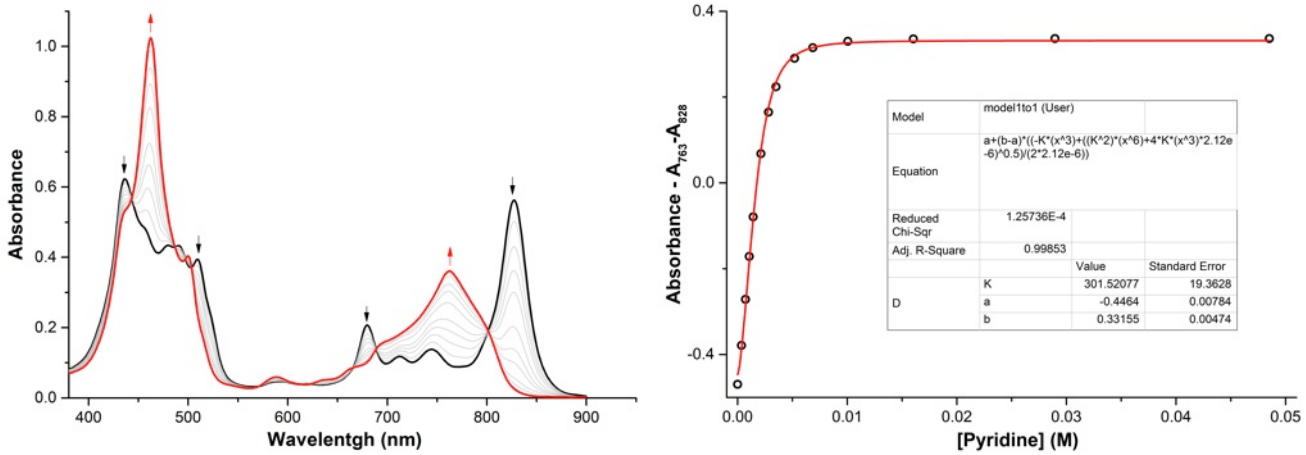

Figure S20. UV/vis/NIR break-up titration of ***l*-P3$_{Zn3}$·T3** ([***l*-P3$_{Zn3}$·T3**] = 2.1 × 10^{-6} M) with pyridine in $CHCl_3$ at 298 K. (a) Changes in absorption upon addition of pyridine. Arrows indicate areas of increasing (red) and decreasing (black) absorption during the titration; (b) Binding isotherm (black dots) derived from the difference of absorption data at λ = 763 and 828 nm and calculated fit (red line, from ORIGIN™ software). Run 1: $\boldsymbol{K_d}$ = 301 ± 20 M^{-2}, R^2 = 0.998.

a) b)

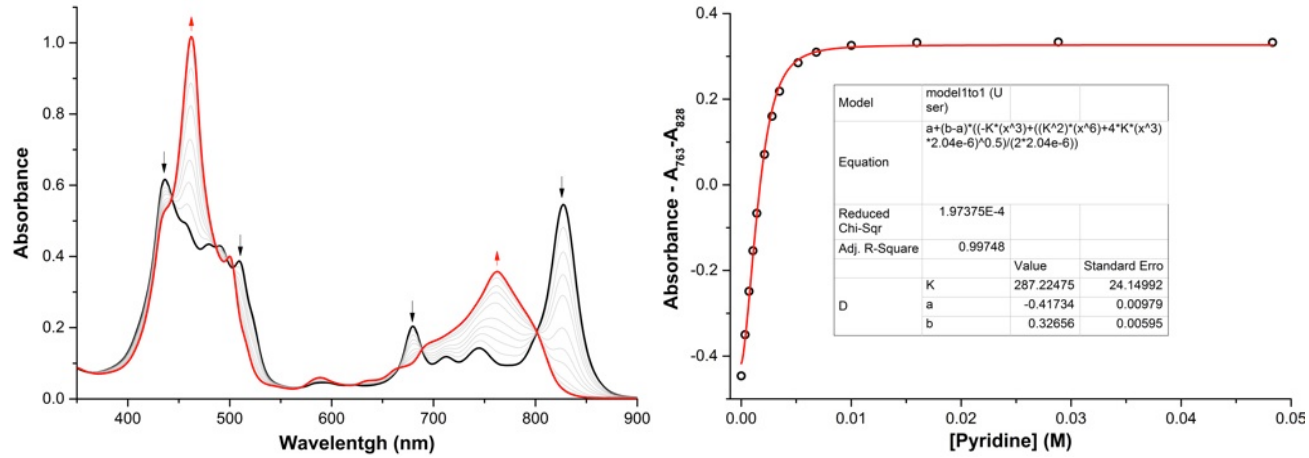

Figure S21. UV/vis/NIR break-up titration of ***l*-P3$_{Zn3}$·T3** ([***l*-P3$_{Zn3}$·T3**] = 2.0 × 10^{-6} M) with pyridine in $CHCl_3$ at 298 K. (a) Changes in absorption upon addition of pyridine. Arrows indicate areas of increasing (red) and decreasing (black) absorption during the titration; (b) Binding isotherm (black dots) derived from the difference of absorption data at λ = 763 and 828 nm and calculated fit (red line, from ORIGIN™ software). Run 2: $\boldsymbol{K_d}$ = 287 ± 24 M^{-2}, R^2 = 0.997.

D2. Determination of K_2 *values by titration of* ***x*****Et-P5** *and* ***x*****-P5** *with* **T3** *and* K_1 *value by titration of* ***l*****-P3$_{ZnH2Zn}$** *with* **T3**

The determination of K_1 allowed us to study the second binding event between complex ***x*****-P5·T3** (and ***x*****Et-P5·T3**) and template **T3** by direct titration. The reference complex ***l*****-P3$_{ZnH2Zn}$·T3** was also studied under the same conditions.

Simulation analysis of the binding isotherms between cross-pentamers ***x*****Et-P5** and ***x*****-P5** and **T3** were analyzed using the software SPECFIT™, using a three-component model: ***x*****Et-P5** / ***x*****Et-P5·T3** / ***x*****Et-P5·(T3)$_2$**. Analysis of the titration curves with SPECFIT™ gives the formation constants of the 1:1 complex ***x*****Et-P5·T3** (K_1) and the 1:2 complex ***x*****Et-P5·(T3)$_2$** ($K_1 \times K_2$). The resulting K_2 are displayed in Table S2 and Figures S22–27.

For linear trimer ***l*****-P3$_{ZnH2Zn}$**, UV/vis/NIR titrations were analyzed by calculating the difference in absorptions and plotted using Origin™ software (Figure S26–27). Due to the relatively weak binding constant between ***l*****-P3$_{ZnH2Zn}$** and **T3**, direct titration experiment could be done to measure the corresponding association constant, K_1, displayed in Table S2.

Table S2. Association constants of cross-pentamers ***x*****Et-P5** and ***x*****-P5** and trimer ***l*****-P3$_{ZnH2Zn}$** with template **T3** (298 K, $CHCl_3$). K_1 values for complexes ***x*****-P5·T3** and ***x*****Et-P5·T3** come from break-up titration experiments, Section D1.

		x**-P5**	***x*****Et-P5**	***l*****-P3$_{ZnH2Zn}$**
K_1	Run 1	*	*	$(3.8 \pm 0.1) \times 10^4$ M^{-1}
	Run 2	*	*	$(2.8 \pm 0.1) \times 10^4$ M^{-1}
	Average	$[(2.8 \pm 0.4) \times 10^8$ $M^{-1}]$*	$[(5.9 \pm 1.2) \times 10^{11}$ $M^{-1}]$*	$(3.3 \pm 0.7) \times 10^4$ M^{-1}
	K_σ	32	32	8
	K_{chem}	$(8.8 \pm 1.3) \times 10^6$ M^{-1}	$(4.1 \pm 1.0) \times 10^5$ M^{-1}	$(4.1 \pm 0.9) \times 10^3$ M^{-1}
	spectra	Fig. S16–17	Fig. S18–19	Fig. S26–27
K_2	Run 1	$(1.9 \pm 0.1) \times 10^5$ M^{-1}	$(3.8 \pm 0.9) \times 10^5$ M^{-1}	
	Run 2	$(1.4 \pm 0.2) \times 10^5$ M^{-1}	$(4.3 \pm 0.9) \times 10^5$	
	Average	$(1.7 \pm 0.3) \times 10^5$ M^{-1}	$(4.1 \pm 1.0) \times 10^5$ M^{-1}	
	K_σ	4	4	
	K_{chem}	$(4.3 \pm 0.7) \times 10^4$ M^{-1}	$(1.0 \pm 0.3) \times 10^5$ M^{-1}	
	spectra	Fig. S22–23	Fig. S24–25	

*fixed values of K_1 from Section D1 were used to analyze the titration data.

Statistical factors are explained in Section D4.

D2a. Binding of ***x*****-P5** *with* **T3**

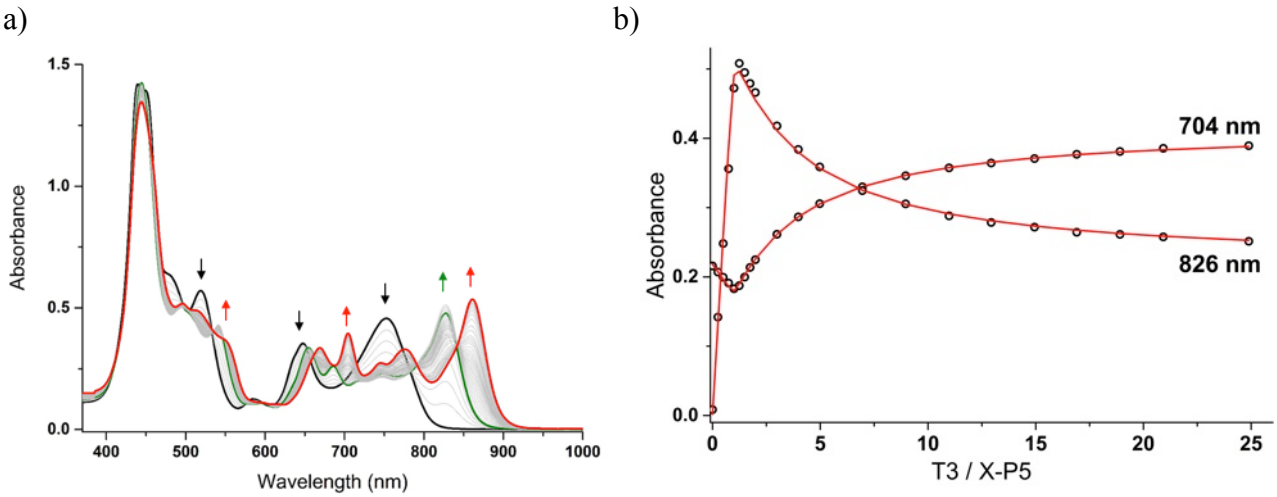

Figure S22. UV/vis/NIR titration of ***x*****-P5** ([***x*****-P5**] = 1.8 × 10^{-6} M) with **T3** in $CHCl_3$ at 298 K. (a) Changes in absorption upon addition of **T3**. Arrows indicate areas of increasing and decreasing absorption during the titration (black for the decrease of free ***x*****-P5**, green for the increase of intermediate 1:1 complex ***x*****-P5·T3** and red for 1:2 complex ***x*****-P5·(T3)$_2$**; (b) Binding isotherm (black dots) derived from absorption data at λ = 704 and 826, nm and calculated fit (red line, from SPECFIT™ software). A square end-point is reached at 1:1 ***x*****-P5·T3** ratio. Run 1: log(***K*$_1$*K*$_2$**) = (13.72 ± 0.03), relative error of fit = 0.9%.

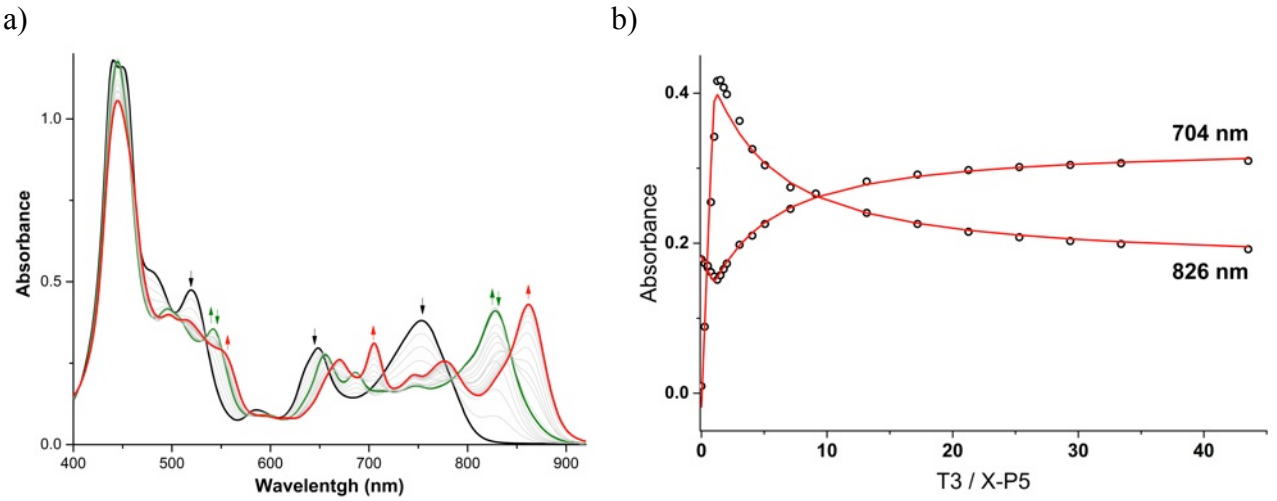

Figure S23. UV/vis/NIR titration of ***x*****-P5** ([***x*****-P5**] = 1.5 × 10^{-6} M) with **T3** in $CHCl_3$ at 298 K. (a) Changes in absorption upon addition of **T3**. Arrows indicate areas of increasing and decreasing absorption during the titration (black for the decrease of free ***x*****-P5**, green for the increase of intermediate 1:1 complex ***x*****-P5·T3** and red for 1:2 complex ***x*****-P5·(T3)$_2$**; (b) Binding isotherm (black dots) derived from absorption data at λ = 704 and 826 nm, and calculated fit (red line, from SPECFIT™ software). A square end-point is reached at 1:1 ***x*****-P5·T3** ratio. Run 2: log(***K*$_1$*K*$_2$**) = (13.61 ± 0.05), relative error of fit = 2.0%.

D2b. Binding of ***x*Et-P5** *with* **T3**

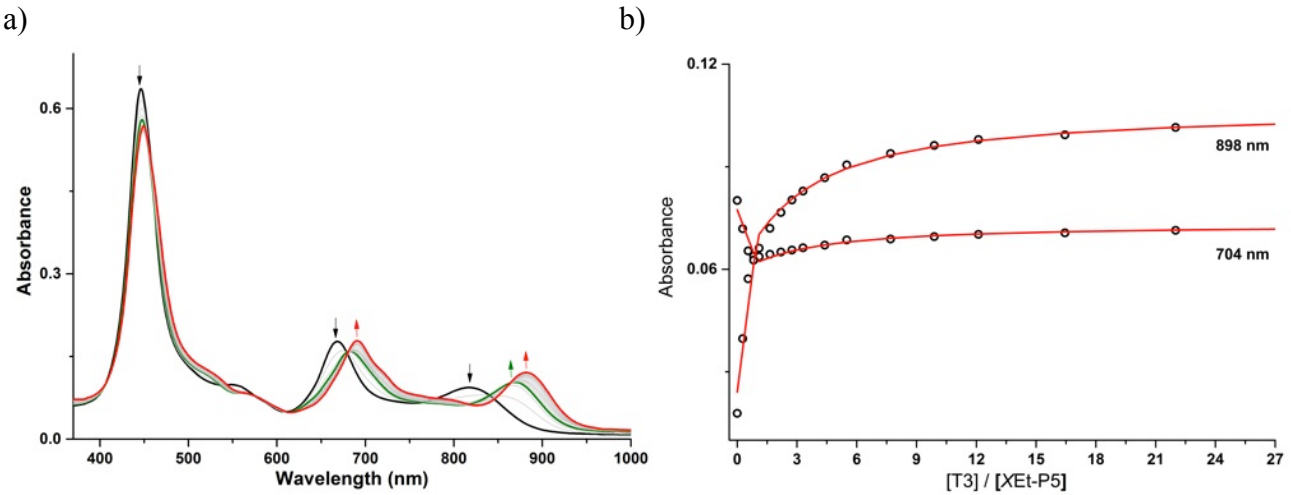

Figure S24. UV/vis/NIR titration of ***x*Et-P5** ([***x*Et-P5**] = 7.6 × 10^{-7} M) with **T3** in $CHCl_3$ at 298 K. (a) Changes in absorption upon addition of **T3**. Arrows indicate areas of increasing and decreasing absorption during the titration (black for the decrease of free ***x*Et-P5**, green for the increase of intermediate 1:1 complex ***x*Et-P5·T3** and red for 1:2 complex ***x*-P5·(T3)$_2$**; (b) Binding isotherm (black dots) derived from absorption data at λ = 898 and 785 nm and corresponding calculated fit (red line, from SPECFIT™ software). A square end-point is reached at 1:1 ***x*-P5·T3** ratio. A square end-point is reached at 1:1 ***x*-P5·T3** ratio. Run 1: log(K_1K_2) = (17.35 ± 0.10), relative error of fit = 1.2%.

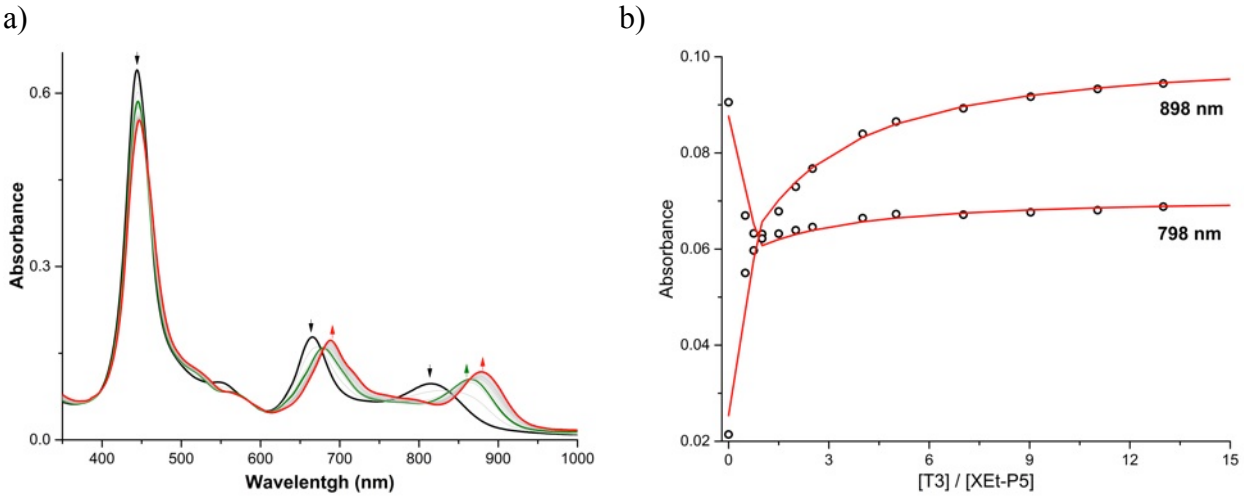

Figure S25. UV/vis/NIR titration of ***x*Et-P5** ([***x*Et-P5**] = 7.5 × 10^{-7} M) with **T3** in $CHCl_3$ at 298 K. (a) Changes in absorption upon addition of **T3**. Arrows indicate areas of increasing and decreasing absorption during the titration (black for the decrease of free ***x*Et-P5**, green for the increase of intermediate 1:1 complex ***x*Et-P5·T3** and red for 1:2 complex ***x*-P5·(T3)$_2$**; (b) Binding isotherm (black dots) derived from absorption data at λ = 898 and 785 nm and corresponding calculated fit (red line, from SPECFIT™ software). A square end-point is reached at 1:1 ***x*-P5·T3** ratio. Run 2: log(K_1K_2) = (17.41 ± 0.09), relative error of fit = 1.1%.

D2c. Binding of ***l*-P3$_{ZnH2Zn}$** *with* **T3**.

a) b)

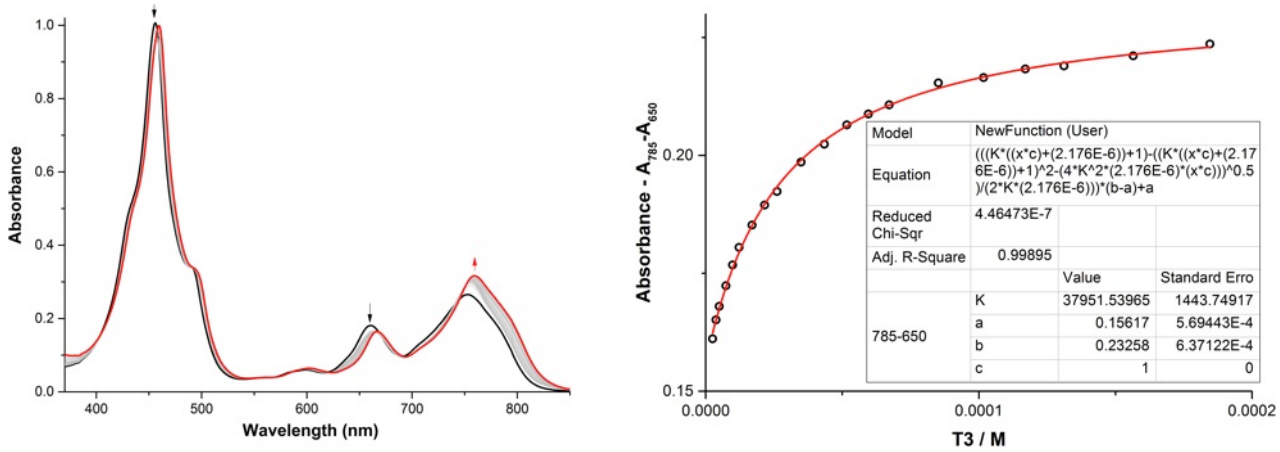

Figure S26. UV/vis/NIR titration of ***l*-P3$_{ZnH2Zn}$** ([***l*-P3$_{ZnH2Zn}$**] = 2.2 × 10^{-6} M) with **T3** in $CHCl_3$ at 298 K. (a) Changes in absorption upon addition of **T3**. Arrows indicate areas of increasing and decreasing absorption during the titration (black for the decrease of free ***l*-P3$_{ZnH2Zn}$** and red for 1:1 complex ***l*-P3$_{ZnH2Zn}$·T3** ; (b) Binding isotherm (black dots) derived from the difference of absorption data at λ = 785 and 650 nm and calculated fit (red line, from ORIGIN™ software). Run 1: $\boldsymbol{K_1}$ = (3.8 ± 1.0) × 10^4 M^{-1}, R^2 = 0.999.

a) b)

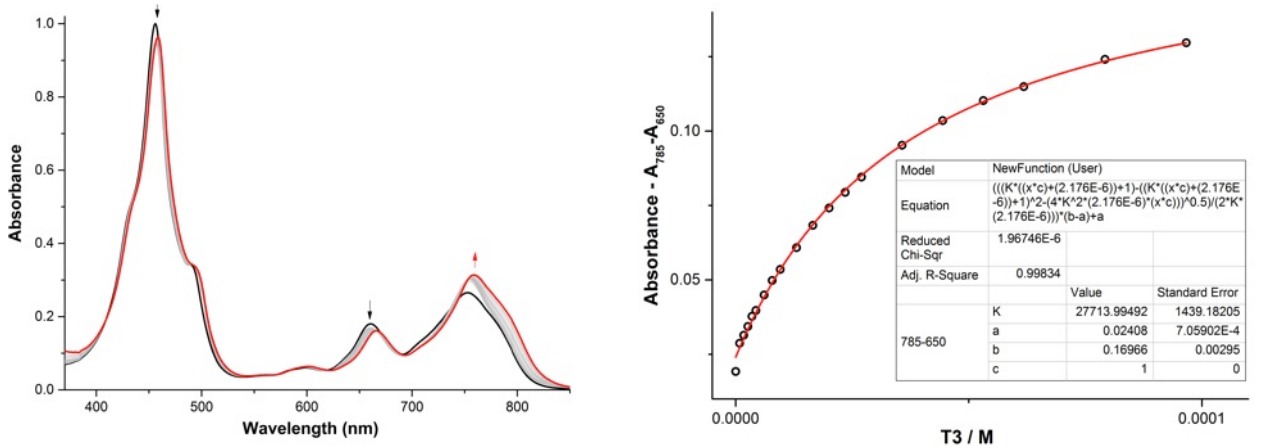

Figure S27. UV/vis/NIR titration of ***l*-P3$_{ZnH2Zn}$** ([***l*-P3$_{ZnH2Zn}$**] = 2.2 × 10^{-6} M) with **T3** in $CHCl_3$ at 298 K. (a) Changes in absorption upon addition of **T3**. Arrows indicate areas of increasing and decreasing absorption during the titration (black for the decrease of free ***l*-P3$_{ZnH2Zn}$** and red for 1:1 complex ***l*-P3$_{ZnH2Zn}$·T3**; (b) Binding isotherm (black dots) derived from the difference of absorption data at λ = 785 and 650 nm and calculated fit (red line, from ORIGIN™ software). Run 2: $\boldsymbol{K_1}$ = (2.8 ± 1.0) × 10^4 M^{-1}, R^2 = 0.998.

D3. Break-up titrations of spiro-nanoring ***s*-P11·(T6)$_2$** *and* ***s*Et-P11·(T6)$_2$** *with quinuclidine.*

Solutions of ***s*-P11·(T6)$_2$** and ***s*Et-P11·(T6)$_2$** in chloroform (containing ca. 0.5% ethanol as stabilizer) were titrated with quinuclidine to displace the **T6** template (at 298 K at constant porphyrin complex concentration by adding porphyrin complex to the ligand stock solution before titrations were started). These UV-vis-NIR titrations show two distinct processes, quantified by the equilibrium constants $\boldsymbol{K_{d1}}$ and $\boldsymbol{K_{d2}}$, which can be interpreted in terms of the thermodynamic cyclic in Figure S28.

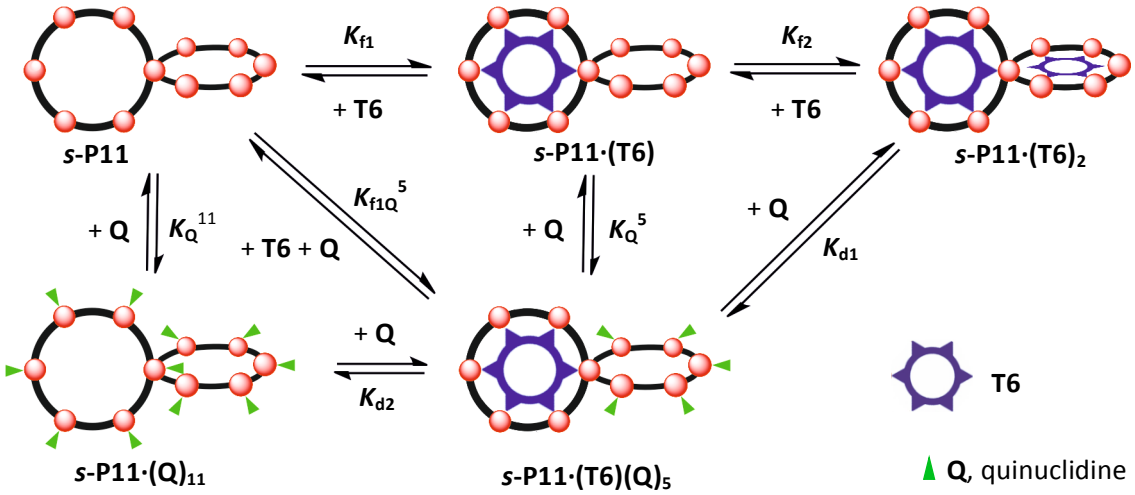

Figure S28. Thermodynamic cycle relating the formation constants of the template complexes ***s*-P11·(T6)** (K_{f1}) and ***s*-P11·(T6)$_2$** (K_{f2}) to the denaturation constants K_{d1} and K_{d2} and the binding constant of each porphyrin unit for quinuclidine. K_Q is the binding constant of one porphyrin unit with quinuclidine, approximated from the binding constant of quinuclidine to cyclic hexamer ***c*-P6** ($K_Q = 3.6 \times 10^5$ M^{-1}). $K_{f1} = K_Q^6/K_{d2}$ and $K_{f2} = K_Q^5/K_{d1}$.

Simulation analysis of these titrations was carried out using the software SPECFIT™ with a three components model: ***s*-P11·(T6)$_2$** / ***s*-P11·(T6)(Q)$_5$** / ***s*-P11·(Q)$_{11}$** with fitting errors of 0.5% for ***s*-P11·(T6)$_2$** and 0.8% for ***s*Et-P11·(T6)$_2$**. The resulting values of $\boldsymbol{K_{f1}}$ and $\boldsymbol{K_{f2}}$ are summarized in Table S3 and Figures S29–S32.

Table S3. Association constants of spiro-nanorings ***s*-P11** and ***s*Et-P11** with template **T6** (in M^{-1}).

		***s*-P11·(T6)$_2$**	***s*Et-P11·(T6)$_2$**
logK_{f1}	Run 1	38.4 ± 0.3	36.6 ± 0.3
	Run 2	37.9 ± 0.3	38.0 ± 0.3
	Average	38.2 ± 0.2	37.3 ± 0.3
	logK_σ	2.89 (see Section D4)	
	logK_{chem}	35.3 ± 0.2	34.4 ± 0.3
logK_{f2}	Run 1	32.5 ± 0.4	29.1 ± 0.4
	Run 2	31.4 ± 0.4	31.7 ± 0.4
	Average	32.0 ± 0.4	30.4 ± 0.4
	logK_σ	2.28 (see Section D4)	
	logK_{chem}	29.7 ± 0.4	28.1 ± 0.4
spectra		Fig. S29–S30	Fig. S31–S32

D3a. Break-up titration of ***s*-P11·(T6)$_2$** *with quinuclidine.*

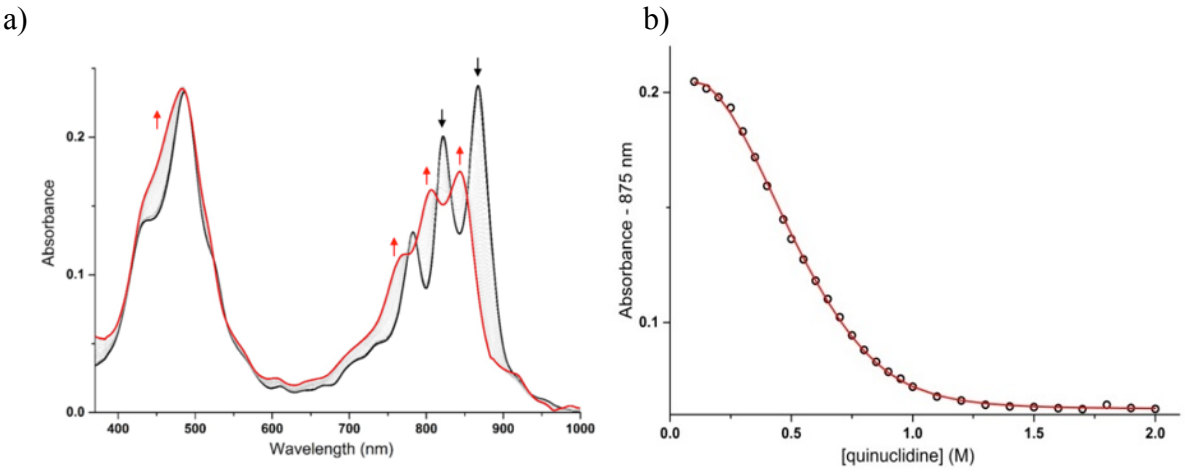

Figure S29. UV/vis/NIR break-up titration of ***s*-P11·(T6)$_2$** ([***s*-P11·(T6)$_2$**] = 4.4 × 10^{-7} M) with quinuclidine in $CHCl_3$ at 298 K. (a) Changes in absorption upon addition of quinuclidine. Arrows indicate regions of increasing (red) and decreasing (black) absorption during the titration; (b) Binding isotherm (black dots) derived from absorption data at λ = 875 nm and calculated fit (red line, from SPECFIT™ software). Run 1: log$\boldsymbol{K}_{f1}$ = 38.4 ± 0.3 and log$\boldsymbol{K}_{f2}$ = 32.5 ± 0.4; relative error of fit = 0.9%.

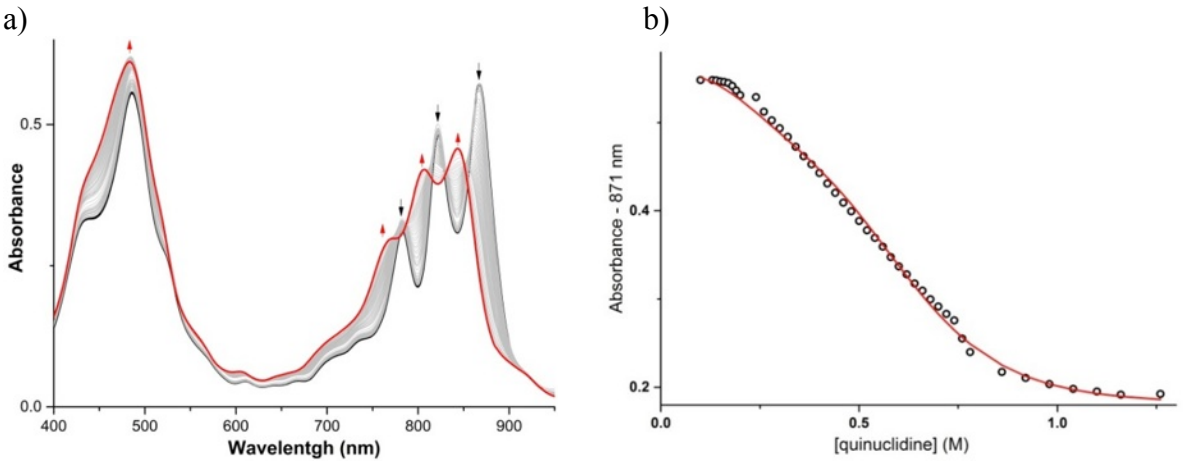

Figure S30. UV/vis/NIR break-up titration of ***s*-P11·(T6)$_2$** ([***s*-P11·(T6)$_2$**] = 7.8 × 10^{-7} M) with quinuclidine in $CHCl_3$ at 298 K. (a) Changes in absorption upon addition of quinuclidine. Arrows indicate regions of increasing (red) and decreasing (black) absorption during the titration; (b) Binding isotherm (black dots) derived from absorption data at λ = 871 nm and calculated fit (red line, from SPECFIT™ software). Run 2: log$\boldsymbol{K}_{f1}$ = 37.9 ± 0.3 and log$\boldsymbol{K}_{f2}$ = 31.4 ± 0.4; relative error of fit = 0.7%.

D3b. Break-up titration of ***s*Et-P11·(T6)$_2$** *with quinuclidine.*

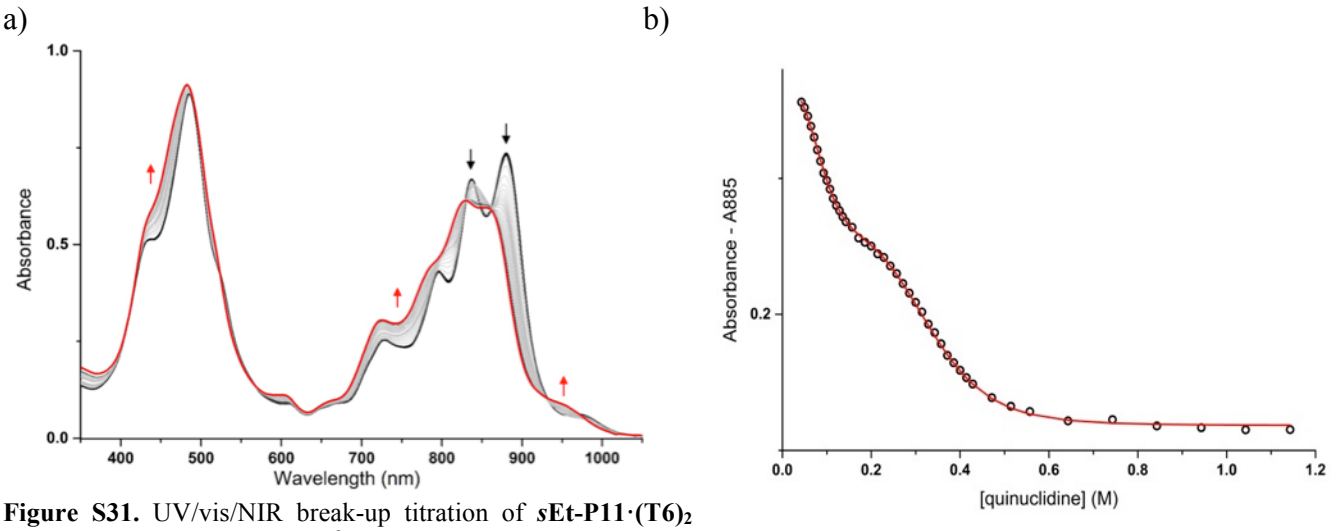

Figure S31. UV/vis/NIR break-up titration of ***s*Et-P11·(T6)$_2$** ([***s*Et-P11·(T6)$_2$**] = 1.0×10^{-6} M) with quinuclidine in $CHCl_3$ at 298 K. (a) Changes in absorption upon addition of quinuclidine. Arrows indicate regions of increasing (red) and decreasing (black) absorption during the titration; (b) Binding isotherm (black dots) derived from absorption data at λ = 885 nm and calculated fit (red line, from SPECFIT™ software). Run 1: log$\boldsymbol{K}_{f1}$ = 36.6 ± 0.3 and log$\boldsymbol{K}_{f2}$ = 29.1 ± 0.4; relative error of fit = 0.3%.

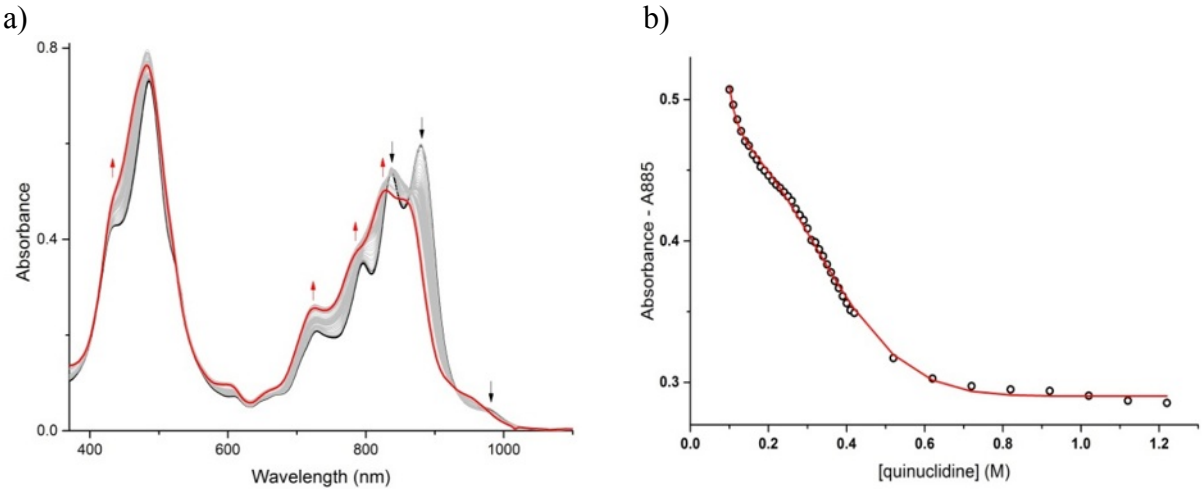

Figure S32. UV/vis/NIR break-up titration of ***s*Et-P11·(T6)$_2$** ([***s*Et-P11·(T6)$_2$**] = 9.1×10^{-7} M) with quinuclidine in $CHCl_3$ at 298 K. (a) Changes in absorption upon addition of quinuclidine. Arrows indicate regions of increasing (red) and decreasing (black) absorption during the titration; (b) Binding isotherm (black dots) derived from absorption data at λ = 885 nm and calculated fit (red line, from SPECFIT™ software). Run 2: log$\boldsymbol{K}_{f1}$ = 38.0 ± 0.3 and log$\boldsymbol{K}_{f2}$ = 31.7 ± 0.4; relative error of fit = 0.6%.

D4. Statistical factors

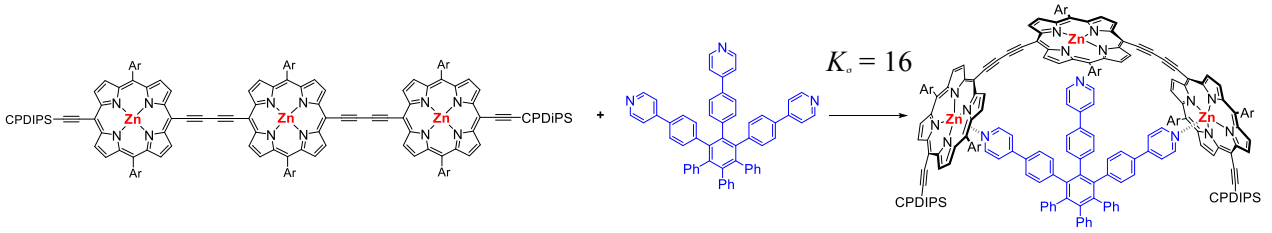

D_{2h}	C_{2v}	C_{2v}
$\sigma_{ext} = 4$	$\sigma_{ext} = 2$	$\sigma_{ext} = 2$
$\sigma_{int} = 2^2$	$\sigma_{int} = 1$	$\sigma_{int} = 1$
$\sigma = 16$	$\sigma = 2$	$\sigma = 2$

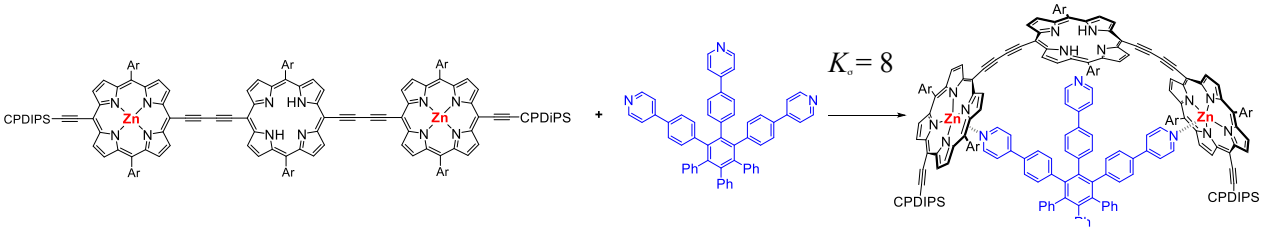

D_{2h}	C_{2v}	C_{2v}
$\sigma_{ext} = 4$	$\sigma_{ext} = 2$	$\sigma_{ext} = 2$
$\sigma_{int} = 2^2$	$\sigma_{int} = 1$	$\sigma_{int} = 2^1$
$\sigma = 16$	$\sigma = 2$	$\sigma = 4$

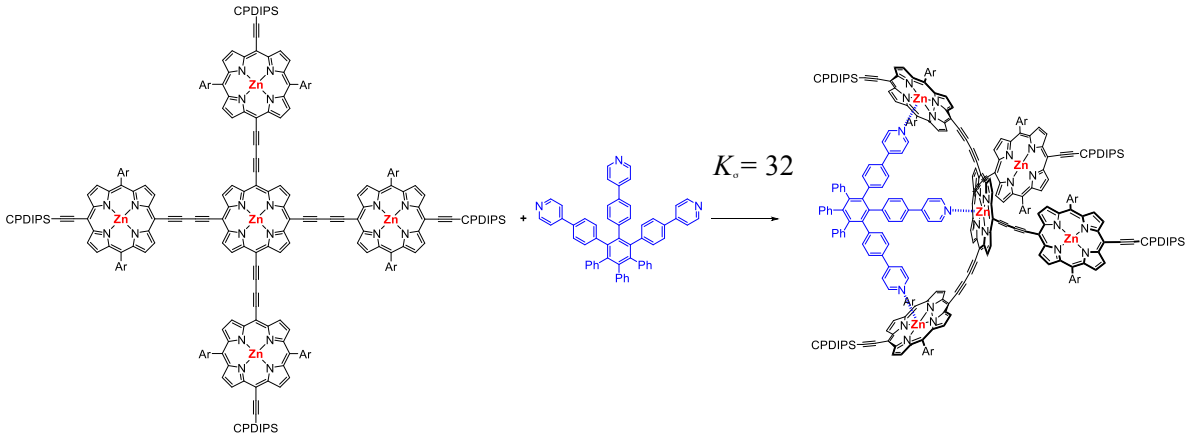

D_{4h}	C_{2v}	C_{2v}
$\sigma_{ext} = 8$	$\sigma_{ext} = 2$	$\sigma_{ext} = 2$
$\sigma_{int} = 2^4$	$\sigma_{int} = 1$	$\sigma_{int} = 2^2$
$\sigma = 128$	$\sigma = 2$	$\sigma = 8$

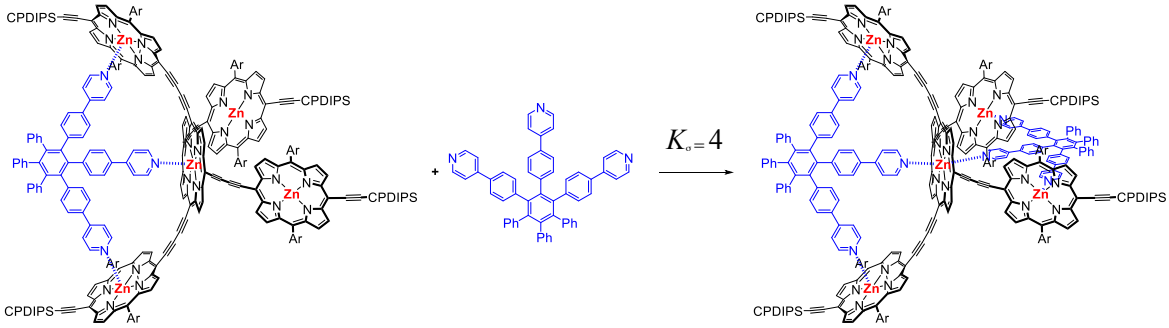

C_{2v}	C_{2v}	D_{2d}
$\sigma_{ext} = 2$	$\sigma_{ext} = 2$	$\sigma_{ext} = 4$
$\sigma_{int} = 2^2$	$\sigma_{int} = 1$	$\sigma_{int} = 1$
$\sigma = 8$	$\sigma = 2$	$\sigma = 4$

Figure S33. Statistical factors for trimers ***l*-P3$_{ZnH2Zn}$** and ***l*-P3$_{Zn3}$** and cross-pentamers ***x*-P5** (statistical factors for ***x*Et-P5** are the same as those of ***x*-P5**).

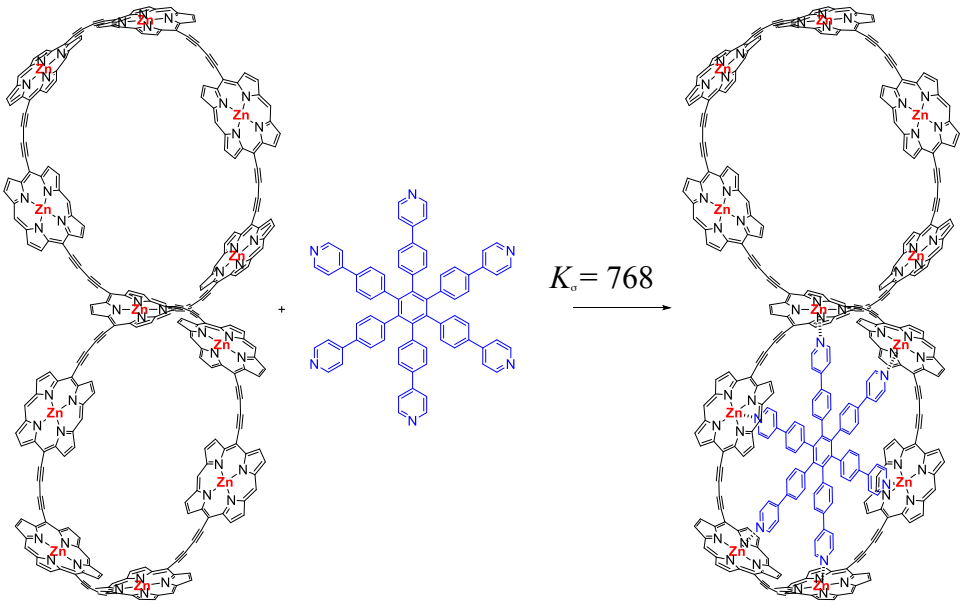

D_{2d}
$\sigma_{ext} = 4$
$\sigma_{int} = 2^{10}$
$\sigma = 4096$

D_{6h}
$\sigma_{ext} = 12$
$\sigma_{int} = 1$
$\sigma = 12$

C_{2v}
$\sigma_{ext} = 2$
$\sigma_{int} = 2^5$
$\sigma = 64$

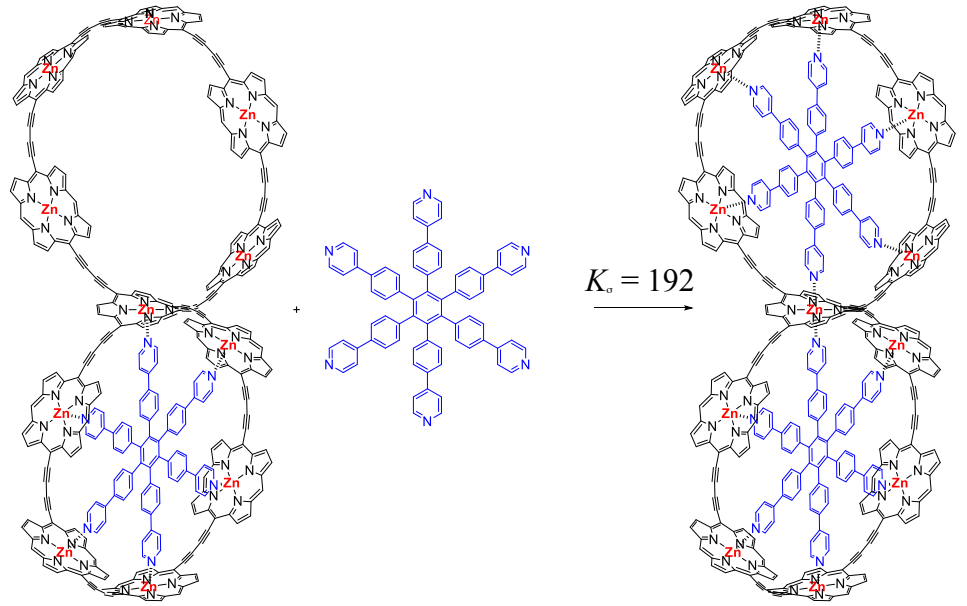

C_{2v}
$\sigma_{ext} = 2$
$\sigma_{int} = 2^5$
$\sigma = 64$

D_{6h}
$\sigma_{ext} = 12$
$\sigma_{int} = 1$
$\sigma = 12$

D_{2d}
$\sigma_{ext} = 4$
$\sigma_{int} = 1$
$\sigma = 4$

Figure 34. Statistical factors for ***s*-P11·(T6)$_2$**. Aromatic groups are omitted for clarity. Statistical factors for ***s*Et-P11·(T6)$_2$** are the same as those for ***s*-P11·(T6)$_2$**.

E. Spectra confirming purity and identity of new compounds

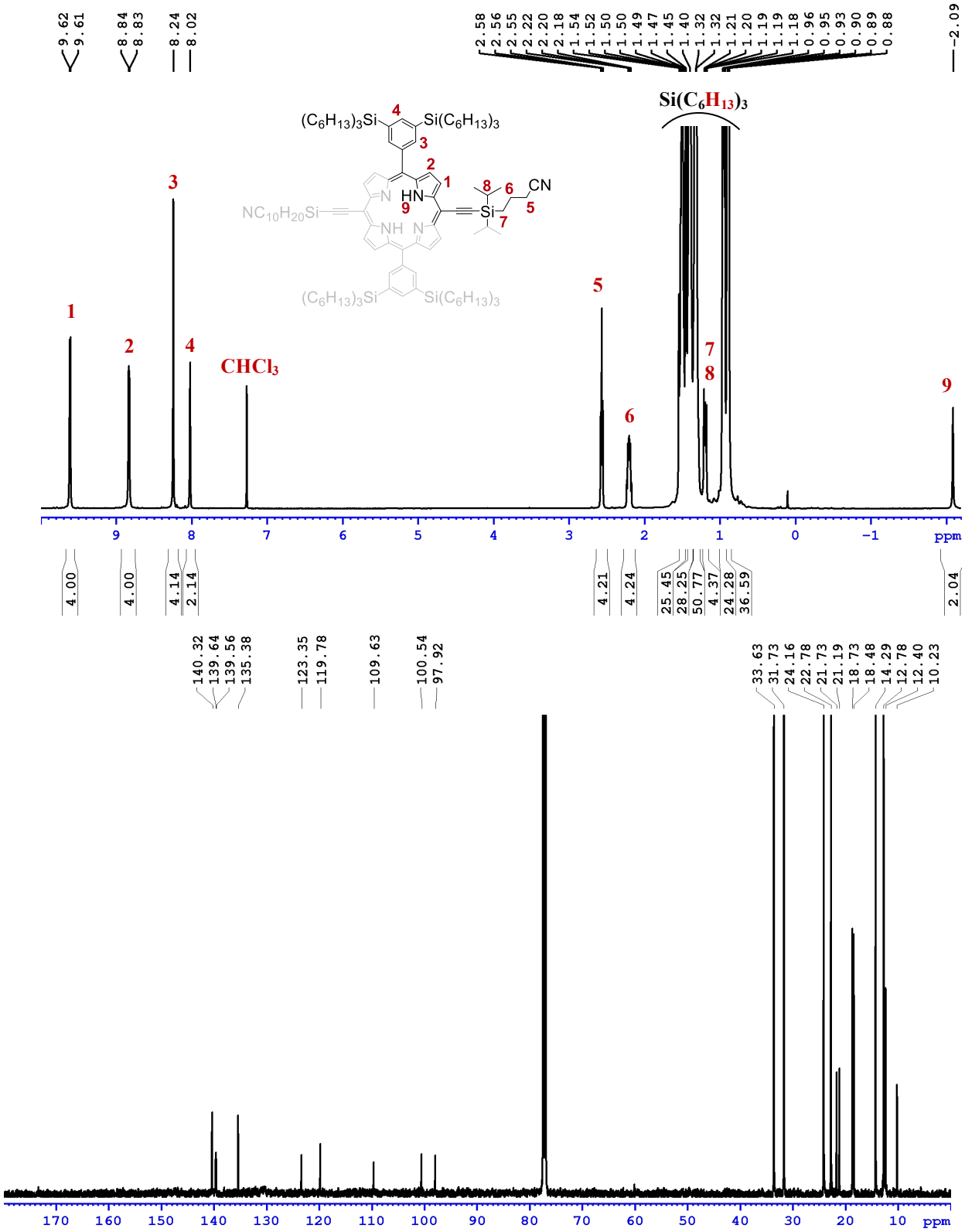

Figure S35. ^{1}H (top) and ^{13}C NMR (bottom) spectra of free-base monomer **P1$_{2H}$** (500 MHz and 125 MHz, $CDCl_3$, 298 K).

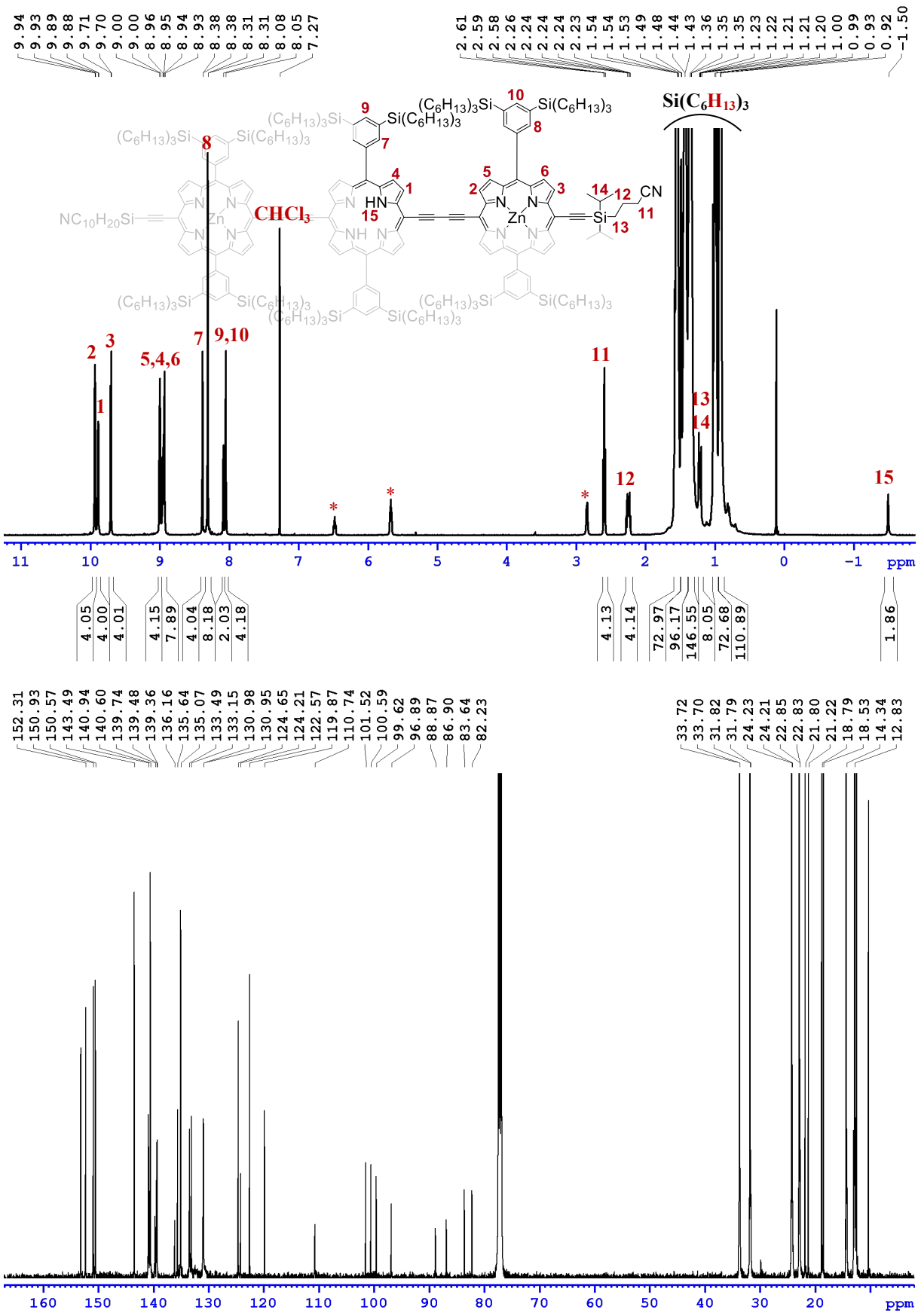

Figure S36. ^{1}H (top, * for pyridine) and ^{13}C NMR (bottom) spectra of trimer ***l*-P3$_{ZnH2Zn}$** (500 MHz and 125 MHz, $CDCl_3$, 298 K).

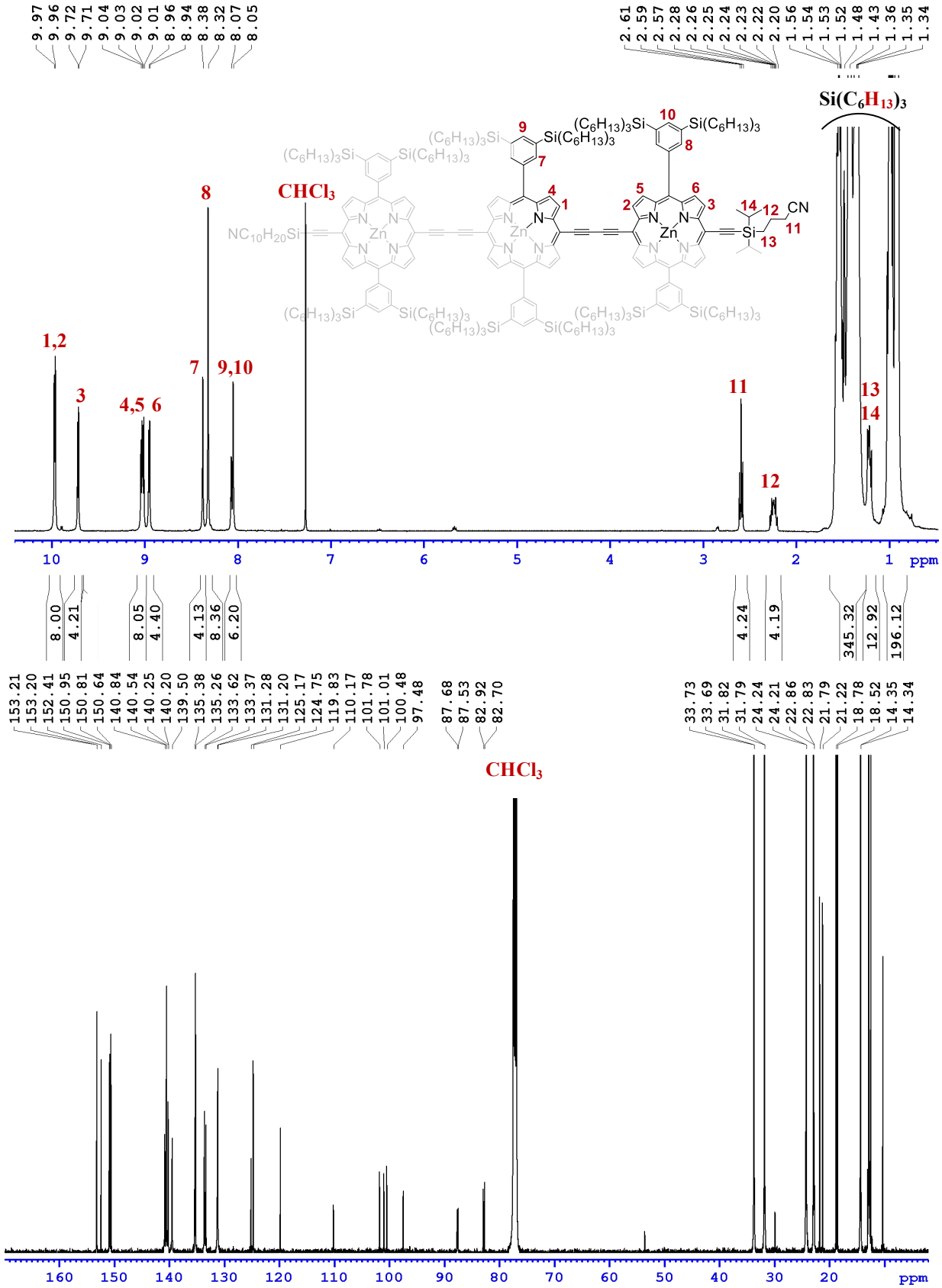

Figure S37. ^{1}H (top) and ^{13}C NMR (bottom) spectra of trimer ***l*-P3$_{THS}$** (400 MHz and 100 MHz, $CDCl_3$, 298 K).

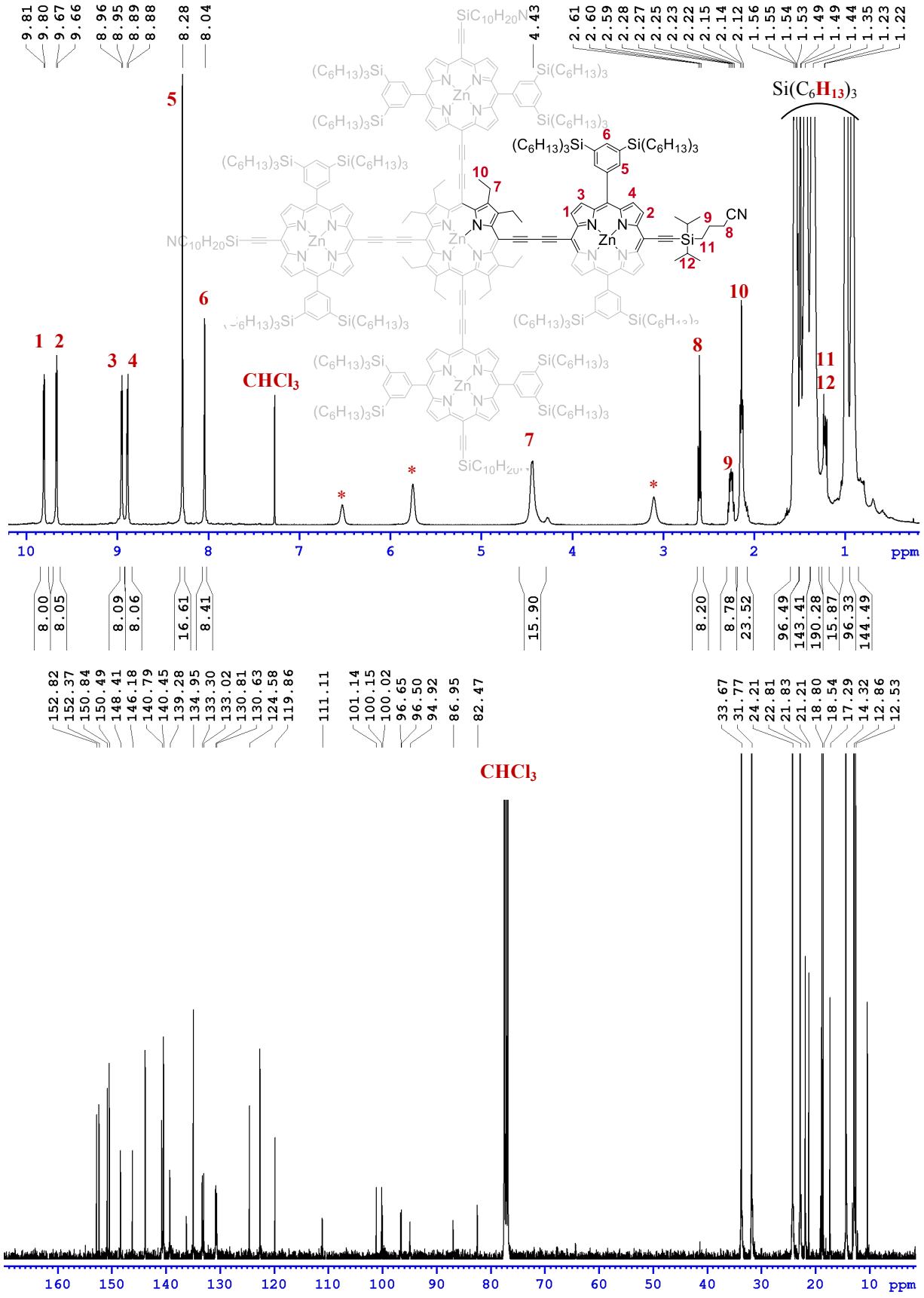

Figure S38. ^{1}H (top, * for pyridine) and ^{13}C NMR (bottom) spectra of pentamer ***x*Et-P5** (500 MHz and 125 MHz, $CDCl_3$, 298 K).

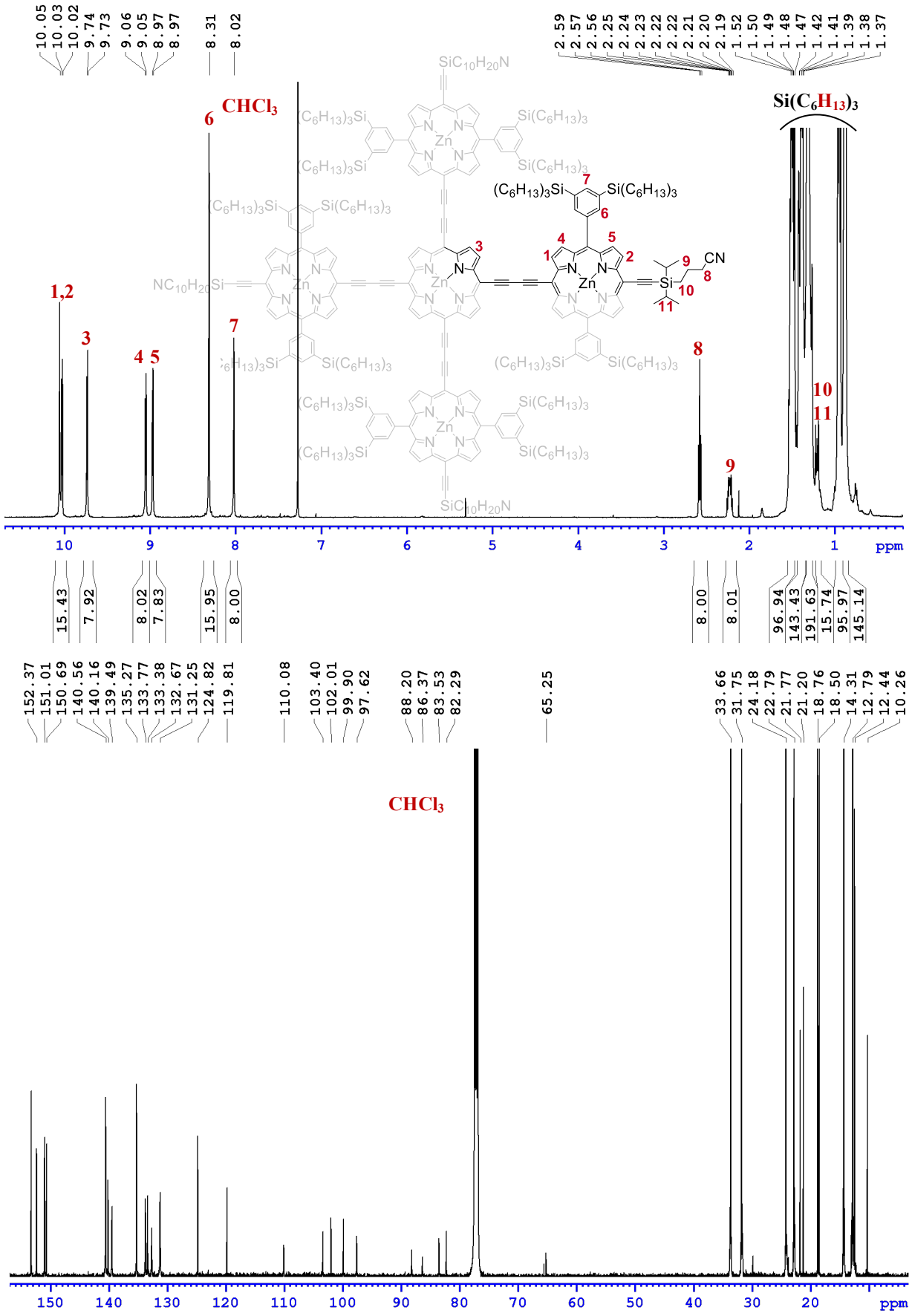

Figure S39. ^{1}H (top) and ^{13}C NMR (bottom) spectra of pentamer ***x*-P5** (500 MHz and 125 MHz, $CDCl_3$, 298 K).

F. Photoluminescence Upconversion Spectroscopy

The photoluminescence (PL) upconversion technique was used to investigate fluorescence dynamics of sample solutions held in quartz cuvettes as described in detail elsewhere.[S10,S11]

An excitation pulse was generated by a mode-locked Ti:Sapphire laser with pulse duration of 100 fs and a repetition rate of 80 MHz. Fluorescence is collected and optically gated in a beta-barium-borate (BBO) crystal by a vertically polarized time-delayed gate beam. The upconverted signal, which consists of sum-frequency photons from the gate pulse and the vertical component of the fluorescence, was collected, dispersed in a monochromator and detected using a nitrogen-cooled CCD. Using a combination of a half-wave plate and a Glan-Thompson polarizer, the polarization of the excitation pulse was varied and fluorescence intensity dynamics were recorded separately for components polarized parallel $I_{\parallel}$ and perpendicular $I_{\perp}$ to the excitation pulse polarization. The fluorescence anisotropy is defined using $\gamma = (I_{\parallel} - I_{\perp})/(I_{\parallel} + 2I_{\perp})$ and calculated from the measured components. The full-width-half-maximum of the instrumental response function was measured to be 270 fs. No anisotropy decay was observed, indicating that any polarization decay must occur within 270 fs for this level of signal-to-noise.

The concentration of the sample solution was on the order of 10^{-4} M. The excitation fluence was kept low (0.32 μJ/cm^2) to avoid fluorescence quenching via exciton-exciton annihilation. The detection wavelength was 915 nm for ***s*-P11·(T6)$_2$** and 987 nm for ***s*Et-P11·(T6)$_2$**.

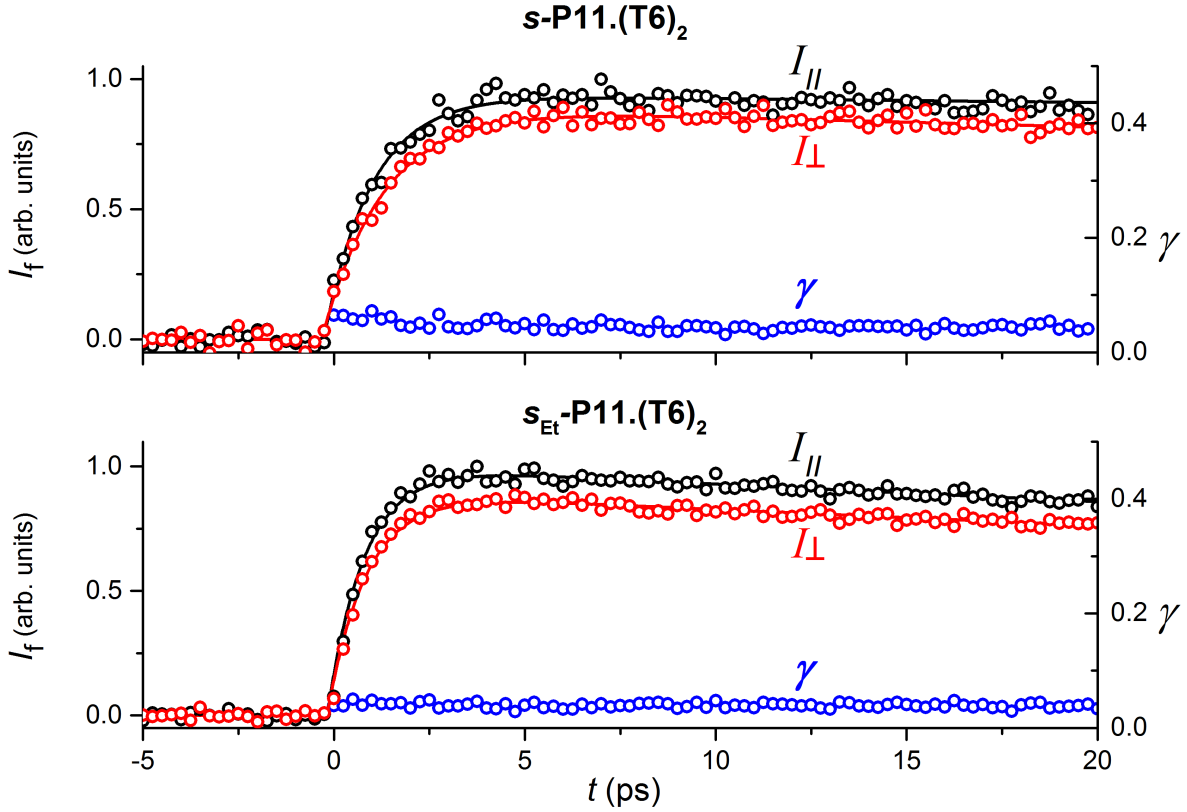

Figure S40. Time-resolved fluorescence decay (components polarized parallel $I_{\parallel}$ and perpendicular $I_{\perp}$ to the excitation pulse polarization, black and red circles, respectively, for experimental data and straight lines for corresponding fitted curves) for ***s*-P11·(T6)$_2$** and ***s*Et-P11·(T6)$_2$** upon excitation at 825 and 835 nm and detection at 915 and 987 nm, respectively, together with the corresponding fluorescence anisotropy dynamics (γ, blue circles) in toluene with 1% pyridine. (The pyridine has no role in this experiment, but it was added because we use 1% pyridine in toluene as a standard solvent, for comparison with other porphyrin oligomers, some of which require pyridine to avoid aggregation.)

G. Anisotropy Modeling

A simple model is used to describe the spiro-nanoring and account for the measured anisotropy.[S12] As illustrated in Figure S41, porphyrin monomer units are assumed to form two smaller loops, each lying in a given plane (the template plane). The angle between the two planes is taken to be 90°. Further assumptions have been made:

1. The initially excited and emitting states are assigned to a pair of two monomers as described below. This is justified, because the anisotropy value does not vary with time over the excitation window and the actual extent of the excitation delocalization does not significantly affect the anisotropy value in such a circular arrangement.
2. The dipole moments are aligned tangentially to the circle the porphyrins are forming, and the porphyrin joining the two loops has two perpendicular dipole moments participating.
3. Each of the 12 dipole moments has equal probability of absorbing and emitting a photon.

The anisotropy can be then be calculated using the following equation:[S12]

$$\gamma = \frac{1}{5}\left(3\langle\cos^2\kappa\rangle - 1\right)$$

where κ denotes the angle between the dipole moments of the absorbing and emitting states. For excitations created at each individual monomer site, $\cos^2\kappa$ with respect to any porphyrin unit on the ring is summed over and the average is taken.

The anisotropy is calculated to be 0.025, which agrees well with the experimental results, that is, 0.03 for ***s*-P11·(T6)$_2$** and 0.04 for ***s*Et-P11·(T6)$_2$**.

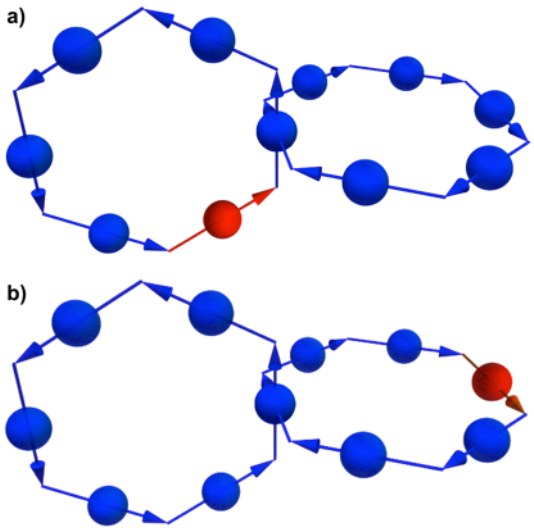

Figure S41. Oscillator distributions on nanorings assumed for PL anisotropy modelling: Circles denote porphyrin monomers and the arrows represent transition dipole moments. Porphyrin units are arranged in two smaller loops lying in two perpendicular planes defined by the templates. a) Initially excited state (red); b) emitting state.

H. References

(S1) Gampp, H.; Maeder, M.; Meyer, C. J.; Zuberbühler, A. D. *Talanta* **1985**, *32*, 257.

(S2) Krivokapic, A.; Cowley, A. R.; Anderson, H. L. *J. Org. Chem.* **2003**, *68*, 1089.

(S3) Anderson, H. L.; Wylie, A. P.; Prout, K. *J. Chem. Soc., Perkin Trans. 1* **1998**, 1607.

(S4) Hogben, H. J.; Sprafke, J. K.; Hoffmann, M.; Pawlicki, M.; Anderson, H. L. *J. Am. Chem. Soc.* **2011**, *133*, 20962.

(S5) Hoffmann, M.; Kärnbratt, J.; Chang, M.-H.; Herz, L. M.; Albinsson, B.; Anderson, H. L. *Angew. Chem. Int. Ed.* **2008**, *47*, 4993.

(S6) Liu, P.; Neuhaus, P.; Kondratuk, D. V.; Balaban, T. S.; Anderson, H. L. *Angew. Chem. Int. Ed.* **2014**, *53*, 7770.

(S7) Benson, S. W. *J. Am. Chem. Soc.* **1958**, *80*, 5151.

(S8) Bailey, W. F.; Monahan, A. S. *J. Chem. Educ.* **1978**, *55*, 489.

(S9) Ercolani, G.; Piguet, C.; Borkovec, M.; Hamacek, J. *J. Phys. Chem. B* **2007**, *111*, 12195.

(S10) Chang, M. H.; Hoeben, F. J. M.; Jonkheijm, P.; Schenning, A. P. H. J.; Meijer, E. W.; Silva, C.; Herz, L. M. *Chem. Phys. Lett.* **2006**, *418*, 196.

(S11) Chang, M. H.; Hoffmann, M.; Anderson, H. L.; Herz, L. M. *J. Am. Chem. Soc.* **2008**, *130*, 10171.

(S12) Gong, J. Q.; Parkinson, P.; Kondratuk, D. V.; Gil-Ramírez, G.; Anderson, H. L.; Herz, L. M. *J. Phys. Chem. C* **2015**, *119*, 6414.